Color octet contribution in exclusive P-wave charmonium decay into octet and decuplet baryons[*]

S.M.H. Wong[1,2,3,4]

[1] School of Physics and Astronomy, University of Minnesota, Minneapolis, MN 55455, USA[a]
[2] Fachbereich Physik, Universität Wuppertal, 42097 Wuppertal, Germany
[3] Institute of Accelerating Systems and Applications (IASA), P.O. Box 17214, 10024 Athens, Greece
[4] Nuclear and Particle Physics Section, University of Athens, Panepistimiopolis, 15771 Athens, Greece

Abstract. In the last years, the need for the color octet state in inclusive P-wave charmonium decay has been firmly established. However, the implications of this in the corresponding exclusive reactions have not been fully recognized. We argue for the necessity of the color octet in P- and higher-wave quarkonium decay. Using a set of phenomenologically constructed baryon wave functions, we consider the χ_J decay into an octet and decuplet baryon–antibaryon pair. By doing so, we subject the wave functions to a test of applicability. We show that the color singlet component alone is insufficient to account for the experimental measurements, and only by including the color octet contribution can the partial theoretical decay widths be brought into the range of the data. By the present and earlier applications of the set of wave functions, these show themselves to be reasonable model wave functions at around the scale $Q^2 \sim 10$–$20\,\mathrm{GeV}^2$.

1 Introduction

In studying strong interaction exclusive processes, a reliable method is the one that bases itself on perturbative QCD, which calls to mind the like of deep inelastic scattering. However, unlike these inclusive reactions where the final states of the hadrons can be summed over, so no explicit knowledge of any of the hadrons is required, in exclusive processes one is usually interested specifically only in a few final hadrons at a time; therefore knowledge of the wave functions of these hadrons is essential. The more accurate picture of a hadron is the Fock state expansion where it is seen as a sum of states with an increasing number of constituents starting from the state with only the valence quarks and/or antiquarks. The probability of the hadron being in any of these states is given by the modulus squared of the wave function associated with each of these states:

$$|B\rangle = \psi_{\text{valence}}|q_1^v q_2^v q_3^v\rangle + \psi_g|q_1^v q_2^v q_3^v g\rangle$$
$$+ \psi_q|q_1^v q_2^v q_3^v q\bar{q}\rangle + \dots$$
$$+ \psi_{g_1 \dots g_M q_1 \dots q_N}|q_1^v q_2^v q_3^v g_1 \dots g_M q_1 \bar{q}_1 \dots q_N \bar{q}_N\rangle$$
$$+ \dots,$$

$$|M\rangle = \psi_{\text{valence}}|q_1^v \bar{q}_2^v\rangle + \psi_g|q_1^v \bar{q}_2^v g\rangle + \psi_q|q_1^v \bar{q}_2^v q\bar{q}\rangle + \dots$$
$$+ \psi_{g_1 \dots g_M q_1 \dots q_N}|q_1^v \bar{q}_2^v g_1 \dots g_M q_1 \bar{q}_1 \dots q_N \bar{q}_N\rangle + \dots$$

[a] Present address.

Because the number of constituents is unlimited, one would require, in general, far too much information before an exclusive process involving even just a few hadrons can be studied. Fortunately as shown by Brodsky and Lepage in [1] in the so-called standard hard scattering approach (SHSA), when a high momentum transfer or high Q^2 is involved in an exclusive process, not only is there factorization and so the process can be partially calculated perturbatively, but also only the lowest valence Fock state wave functions of the hadrons are needed. The higher Fock states are suppressed by the large Q^2. Thus the large momentum transfer acts as a filter to let pass only the lowest state of the hadrons. It has also been proved by Duncan and Mueller [2] that these points are also true in quarkonium decay with a large timelike momentum transfer.

Most recent developments in inclusive quarkonium physics have seen, on the other hand, the need for the next higher Fock state in P-wave quarkonia [3,4], the so-called color octet, where the heavy $Q\bar{Q}$ pair is in a color octet rather than the usual color singlet as in the valence state. This higher state is made up of the $Q\bar{Q}$ plus a gluon. This is special to heavy quarkonium and can be understood in terms of a suppression on the level of the wave function due to angular momentum as we will explain in later sections. The advance in inclusive processes involving quarkonia has yet to fully bring about the same level of understanding in the corresponding exclusive process. Part of our goals in this paper is therefore to show that the color octet is not only important in inclusive but also

in exclusive processes. We will achieve this by studying P-wave χ_J decay into baryon–antibaryon.

As mentioned above, knowledge of the hadronic wave functions is very important. Even in large momentum transfer processes, valence wave functions are still necessary. Since bound state wave equations in QCD are too hard to solve, other ways to obtain the solutions or the hadronic wave functions must be used. One way is via QCD moment sum rules [5–7]. However, it has been shown in [8] that a perturbative calculation of the proton magnetic form factor using the range of existing nucleon distribution amplitudes thus obtained gives results that are, on the average, at least a factor of two below the experimental measurements in the range of Q^2 up to $50\,\mathrm{GeV}^2$. It is therefore clear that the perturbative contribution is not dominant in this rather low range of Q^2. This has also been pointed out in [9]. Nucleon wave functions constructed from such distribution amplitudes are, therefore, not applicable in reactions with values of Q^2 far from asymptotic, not to mention the fact that there might be ambiguities in the distribution amplitudes determined in this way.

In order to obtain a nucleon wave function that is suitable for application at values as low as $10\,\mathrm{GeV}^2$, the usually neglected but nevertheless ever present soft overlap between the final and initial nucleon wave function contribution to the magnetic form factor is taken to make up for the difference between the perturbative contribution and the experimental measurements. It was shown in [10] that a nucleon model wave function could indeed be constructed this way, using constraints from the valence quark distribution, the J/ψ decay width into a nucleon–antinucleon pair, and existing data on the nucleon electromagnetic form factor. We are motivated in this regard to show that the above construction of a model nucleon wave function and its generalization to other octet and decuplet baryons [11] provides a reasonable description of the baryonic valence Fock state wave functions at around $10\,\mathrm{GeV}^2$. To do that we must apply these wave functions to exclusive processes. Our investigation will allow us to study this as well as the color octet contribution.

Since in χ_J decay into a baryon–antibaryon pair only a nucleon–antinucleon pair in the final state has been measured, our calculations will show first that the color singlet contribution alone is not sufficient and by including that of the octet, the partial decay width can be brought into reasonable agreement with experiment. Then with the generalization of the nucleon wave function to the whole flavor octet and decuplet multiplet, we can provide predictions for the widths of the χ_J decay into other baryon pairs.

The paper is organized as follows. First we review briefly in Sect. 2 the angular momentum suppression in the P-wave wave function, and in Sect. 3 we give a theoretical argument for the inclusion of the color octet component in the exclusive decay process. In Sect. 4, the set of phenomenologically constructed baryon wave functions will be presented and explained before we use the improved modified hard scattering scheme (MHSA) of Botts, Li and Sterman [12,13] to obtain the singlet contribution

in Sect. 5 and 6. The results will be compared to experiment. In Sect. 7, our method of obtaining a wave function of the higher color octet state of the χ_J and the Feynman graphs of the decay process will be given. The details in constructing the octet contribution to the hard perturbative part T_H will be explained in Sect. 8. The actual calculation and the results are in Sect. 9 and 10, respectively. In the appendices, all essential details of the calculation, the propagators and the numerators of the graphs used in Sect. 9 are given.

2 Angular momentum suppression of charmonium wavefunctions

In this section, we show that there is a suppression of the charmonium wave function due simply to the angular momentum of the heavy quark–antiquark system. This has important consequences as we will see in the next section, where we briefly review the more detailed argument given in [14]. The hadronic decay of charmonium is through the annihilation of the charm with the anticharm, which is a short distance process because of the heavy charmonium mass. The annihilation size L is roughly given by $L \sim 1/M$, the inverse of the heavy mass M. The charmonium wave function, which must enter the decay probability amplitude, is therefore needed predominantly at $L \sim 1/M \sim 0$ for heavy charmonium decay. That is, we have $\psi_\mathrm{S}(L) \sim \psi_\mathrm{S}(0)$ for the wave function at the spatial origin. This is the case for S-wave charmonium such as η_c or J/ψ. For P-wave charmonium, the wave function in fact vanishes at the origin, so instead one has to expand the wave function around the origin. What enters the probability amplitude is actually $\psi_\mathrm{P}(L) \sim L\,\psi_\mathrm{P}'(L) \sim L\,\psi_\mathrm{P}'(0)$. Going to momentum space, the probability amplitudes for S- and P-wave decay include the wave function of the form

$$\text{S-wave:} \qquad \psi_\mathrm{S}(L) \qquad\qquad \longrightarrow \tilde{\psi}_\mathrm{S}(k),$$

$$\text{P-wave:} \qquad \psi_\mathrm{P}(L) \sim L\psi_\mathrm{P}'(0) \longrightarrow \frac{k}{M}\tilde{\psi}_\mathrm{P}(k),$$

respectively, where k is the internal momentum of the charmonium, and the average value $\langle k \rangle$ is of the order of a few hundreds MeV. So it becomes clear that P-wave decay is suppressed by $1/M$ in comparison to S-wave at the level of the wave function. This suppression is one of the reasons why the color octet is necessary for P-wave inclusive decay. We will see in the next section that it also provides the reason for its inclusion in exclusive decays.

3 Comparison of the large scale dependence of color singlet and color octet

The simplest scheme to calculate the charmonium partial decay width that is built on the solid basis of perturbative QCD is the hard scattering approach of Brodsky and Lepage [1]. In this scheme, the decay probability amplitude can be factorized into a hard and soft part and is given by

a convolution of hadronic distribution amplitudes, the ϕ's, and the hard perturbative part T_{H}. For the decay of χ_J into a baryon–antibaryon, or more specifically a nucleon–antinucleon, this is

$$\mathcal{M} \sim f_{\chi_J} \phi_{\chi_J}(x) \otimes f_N \phi_N(x) \otimes f_{\bar N} \phi_{\bar N}(x) \otimes T_{\mathrm{H}}(x). \quad (1)$$

Since the distribution amplitudes are nothing but the hadronic wave functions with their internal transverse momenta being integrated over, there is still the decay constant f accompanying each distribution amplitude. While the amplitudes themselves are dimensionless, the decay constants f carry different mass dimensions, depending on the original hadronic wave functions. From the fact that the partial decay width is given by

$$\Gamma_{\mathrm{partial}} \sim |\mathcal{M}|^2/M, \quad (2)$$

and there is only one mass scale M in the process, namely the heavy charmonium mass, we can use power counting on (1) to compare, once the mass dimensions of the decay constants are known, the color singlet and octet contribution to the decay width and hence their relative importance to a particular hadronic decay process. For the determination of the mass dimension of f, we refer to [14].

Examining (1), we see that the decay constant of the valence Fock state of the nucleon f_N and the color octet charmonium decay constant $f_{\chi_J}^{(8)}$ are both 3-particle wave functions. Therefore, they must be of mass dimension two. The color singlet decay constant $f_{\chi_J}^{(1)}$, on the other hand, is a 2-particle wave function so it should be of dimension one. However, the fact that χ_J are P-wave charmonia increases this to dimension two. The only remaining quantity in (1) that has a dimension is T_{H}, which contains a hidden power of M. This power must make up the right dimension for $\mathcal{M}$, which must be dimension one in view of (2). So we can now collect all the dimensional quantities in the color singlet and octet probability amplitudes and determine their dependence on the large scale M. We get

$$\mathcal{M}^{(1)} \sim M \frac{f_{\chi_J}^{(1)}}{M^2} \left(\frac{f_N}{M^2} \right)^2 \sim \frac{1}{M^5}, \quad (3)$$

$$\mathcal{M}^{(8)} \sim M \frac{f_{\chi_J}^{(8)}}{M^2} \left(\frac{f_N}{M^2} \right)^2 \sim \frac{1}{M^5}. \quad (4)$$

It is now clear that both the singlet and octet contribution for the P-wave χ_J are weighted by the inverse fifth power of the charmonium mass. The color octet, although a higher Fock state of the charmonium, is not suppressed by the large scale of the decay process in relation to the valence singlet state.

If there were no suppression at the level of the P-wave wave function as explained in the previous section, for example in the case of J/ψ decay, the dependence of the singlet contribution on M would have been $1/M^4$. Therefore, the color octet contribution can be neglected in the decay of a S-wave but not that of a P-wave charmonium. For more details of the argument above, one can consult [14].

4 Baryon wavefunctions

4.1 Octet baryons

As mentioned in Sect. 1, most model wave functions constructed from QCD moment sum rules [5–7,15–17] lead to rather unsatisfactory distribution amplitudes at moderate Q^2 [8,9] and they certainly do not describe the experimental data. A different model wave function suitable for the application at such low momentum transfers was constructed in [10]. This construction is based on the following form of the nucleon wave function,

$$|p, +\rangle = \frac{\varepsilon_{a_1 a_2 a_3}}{\sqrt{3!}} \int [\mathrm{d}x][\mathrm{d}^2 \boldsymbol{k}_\perp]$$
$$\times \left\{ \Psi_{123}^N |u_+^{a_1} u_-^{a_2} d_+^{a_3}\rangle + \Psi_{213}^N |u_-^{a_1} u_+^{a_2} d_+^{a_3}\rangle \right.$$
$$\left. - (\Psi_{132}^N + \Psi_{231}^N)|u_+^{a_1} u_+^{a_2} d_-^{a_3}\rangle \right\}. \quad (5)$$

which is the most general of the nucleon wave function with zero orbital angular momentum [18]. The nucleon, being an isospin doublet, is also the lowest energy state of the baryons and it is therefore reasonable to assume that it has zero orbital angular momentum. These conditions permit the presence of only one scalar function Ψ, which is a function of the light-cone momentum fractions x_i and the internal transverse momentum $\boldsymbol{k}_{\perp i}$ of the nucleon. In the notation of [10], it is given in terms of the nucleon decay constant, or equivalently the wave function at the origin f_N, the distribution amplitude ϕ_{123} and the function containing the transverse momentum dependence Ω_N, by

$$\Psi_{123}(x, \boldsymbol{k}_\perp) = \Psi(x_1, x_2, x_3; \boldsymbol{k}_{\perp 1}, \boldsymbol{k}_{\perp 2}, \boldsymbol{k}_{\perp 3})$$
$$= \frac{1}{8\sqrt{3!}} f_N(\mu_F) \phi_{123}^N(x, \mu_F) \Omega_N(x, \boldsymbol{k}_\perp), \quad (6)$$

and

$$[\mathrm{d}x] = \prod_{i=1}^{3} \mathrm{d}x_i\, \delta \left(1 - \sum_{i=1}^{3} x_i \right), \quad (7)$$

$$[\mathrm{d}^2 \boldsymbol{k}_\perp] = \frac{1}{(16\pi^3)^2} \prod_{i=1}^{3} \mathrm{d}^2 \boldsymbol{k}_{\perp i} \delta^{(2)} \left(\sum_{i=1}^{3} \boldsymbol{k}_{\perp i} \right), \quad (8)$$

are the usual constrained integration measures over the momentum fractions and the internal transverse momenta. The function Ω_N is conveniently taken to be of Gaussion form:

$$\Omega_N(x, \boldsymbol{k}_\perp) = (16\pi^2)^2 \frac{a_N^4}{x_1 x_2 x_3}$$
$$\times \exp \left[-a_N^2 \sum_{i=1}^{3} \boldsymbol{k}_{\perp i}{}^2 / x_i \right]. \quad (9)$$

where a_N is a transverse size parameter which was fitted with the decay constant f_N to the experimental data by the procedure described in [10] to be $a_N = 0.75\,\mathrm{GeV}^{-1}$ and $f_N(\mu_0) = 6.64 \times 10^{-3}\,\mathrm{GeV}^2$ at the reference scale $\mu_0 = 1.0\,\mathrm{GeV}$.

The distribution amplitude ϕ_{123} as well as the decay constant have to be evolved to the factorization scale μ_F of the process in question. In terms of the eigenstates of the evolution equation, the effect of the evolution is to change the coefficients of each eigenstate by a certain power of the log of the relevant scale. The nucleon distribution amplitude expressed in the Appell polynomial eigenbasis is

$$
\begin{aligned}
\phi_{123}^N(x,\mu_F) &= \phi_{\mathrm{AS}}(x)\left[1 + \sum_{n=1}^{\infty} B_n^N(\mu_F)\,\tilde{\phi}_{123}^n(x,\mu_F)\right] \\
&= \phi_{\mathrm{AS}}(x)\left[1 + \frac{3}{4}\tilde{\phi}_{123}^1(x) + \frac{1}{4}\tilde{\phi}_{123}^2(x)\right] \\
&= 60x_1 x_2 x_3[1 + 3x_1].
\end{aligned}
\tag{10}
$$

Under a change of scale both the coefficients B_n^N of the expansion and the decay constant are scaled by the following factors of logarithm of the relevant scale μ_F:

$$
f_N(\mu_F) = f_N(\mu_0)\left(\frac{\ln(\mu_0/\Lambda_{\mathrm{QCD}})}{\ln(\mu_F/\Lambda_{\mathrm{QCD}})}\right)^{2/3\beta_0},
\tag{11}
$$

$$
B_n^N(\mu_F) = B_n^N(\mu_0)\left(\frac{\ln(\mu_0/\Lambda_{\mathrm{QCD}})}{\ln(\mu_F/\Lambda_{\mathrm{QCD}})}\right)^{\tilde{\gamma}_n/\beta_0},
\tag{12}
$$

where the $\tilde{\gamma}_n$ are the reduced anomalous dimensions and β_0 is the first coefficient of the β function. The last line in (10) is the expression for ϕ_{123}^N at the scale $\mu_F = \mu_0$.

As shown in [11], the form of the nucleon wave function need not be restricted to the SU(2) isospin doublet. On the contrary, one can extend it to the complete SU(3) flavor octet. The simplest way to do this, with SU(3) flavor symmetry breaking by the heavier strange quark mass taken into account, is to assume that the complete baryon octet shares the same octet transverse size parameter, $a_{B_8} = 0.75$ GeV and the octet decay constant, $f_{B_8} = 6.64 \times 10^{-3}$ GeV^2. Then the flavor symmetry breaking effects are all put into the octet distribution amplitudes $\phi_{123}^{B_8}$ and they manifest themselves as an uneven distribution of the light-cone momentum fractions amongst the valence quarks. As shown in [11], introducing an additional exponential dependence on the strange constituent quark mass m_s, of the form

$$
\exp\left(-\frac{a_{B_8}^2 m_s^2}{x_j}\right),
\tag{13}
$$

in the distribution amplitude for each strange quark with label j suffices for the purpose. Using several different values of m_s, representative sets of the expansion coefficients B^{B_8} of the octet distribution amplitudes $\phi_{123}^{B_8}$ can be obtained. Set 3 in [11], obtained with $m_s = 350$ MeV, is most promising and will be used in the following investigations.

The octet baryon wave functions with positive helicities can then be expressed as follows:

$$
|B_8,+\rangle = \frac{\varepsilon_{a_1 a_2 a_3}}{\sqrt{3!}}\int[\mathrm{d}x][\mathrm{d}^2\boldsymbol{k}_\perp]
$$
$$
\times\{\Psi_{123}^{B_8}|f_{1+}^{a_1}f_{1-}^{a_2}f_{2+}^{a_3}\rangle + \Psi_{213}^{B_8}|f_{1-}^{a_1}f_{1+}^{a_2}f_{2+}^{a_3}\rangle
$$

$$
- (\Psi_{132}^{B_8}+\Psi_{231}^{B_8})|f_{1+}^{a_1}f_{1+}^{a_2}f_{2-}^{a_3}\rangle\},
\tag{14}
$$

$$
|\Lambda,+\rangle = \frac{\varepsilon_{a_1 a_2 a_3}}{\sqrt{2}}\int[\mathrm{d}x][\mathrm{d}^2\boldsymbol{k}_\perp]
$$
$$
\times\{\Psi_{123}^{\Lambda}|u_+^{a_1}d_-^{a_2}s_+^{a_3}\rangle - \Psi_{213}^{\Lambda}|u_-^{a_1}d_+^{a_2}s_+^{a_3}\rangle
$$
$$
+ (\Psi_{132}^{\Lambda}-\Psi_{231}^{\Lambda})|u_+^{a_1}d_+^{a_2}s_-^{a_3}\rangle\},
\tag{15}
$$

where $f_j^{a_i}$ stands for the quark flavor of quark j with color a_i and $\Psi_{123}^{B_8}$ is the corresponding scalar functions in (6) of the octet baryons. The Λ is a slightly different member of the flavor octet multiplet. Being an isospin singlet, it has to vanish under the action of SU(2)$_{\mathrm{isospin}}$ and therefore has different signs between the different wave function components.

4.2 Decuplet baryons

As we mentioned in the Introduction, our interest in this investigation is the χ_J decay into a baryon–antibaryon pair. Unlike the octet baryon–antibaryon which can be coupled only to spin $S = 1$, a decuplet baryon–antibaryon pair can coupled to $S = 2$ as well. This leads to the interesting potential possibility of χ_2 with $S_z = 2$ to decay into a coupled decuplet baryon pair with the same total third component of the spin. However, within perturbative QCD, this is not possible due to quark and gluon coupling via a vector coupling. This results in the well-known helicity conservation or helicity sum rule, which forces the outgoing baryon–antibaryon pair to have zero total helicity [19]. Or in other words, they must be in a total spin one state. For the same reason, χ_0 decay into baryon–antibaryon is forbidden. Therefore for the decuplet baryons, all we need are the helicity $+1$ decuplet baryon wave functions.

Starting from the Δ^{++}, the simplest distribution amplitude which is symmetric between the three u-quarks is the asymptotic distribution amplitude $\phi_{\mathrm{AS}}(x)$. Using this as the starting point, one can likewise generalize to the whole decuplet baryon multiplet and introduce SU(3) flavor symmetry breaking in the same manner as in Sect. 4.1 by using an exponential m_s dependence. This again yields several sets of representative expansion coefficients $B_n^{B_{10}}$ for the decuplet baryon distribution amplitudes $\phi_{123}^{B_{10}}(x)$. They are listed in Table 1. The decuplet wave functions can be expressed in a similar fashion as before:

$$
|\Delta^{++},+\rangle = \frac{\varepsilon_{a_1 a_2 a_3}}{\sqrt{2}}\int[\mathrm{d}x][\mathrm{d}^2\boldsymbol{k}_\perp]
$$
$$
\times\Psi_{123}^{\Delta}|u_+^{a_1}u_-^{a_2}u_+^{a_3}\rangle,
\tag{16}
$$

$$
|B_{10},+\rangle = \frac{\varepsilon_{a_1 a_2 a_3}}{\sqrt{3!}}\int[\mathrm{d}x][\mathrm{d}^2\boldsymbol{k}_\perp]
$$
$$
\times\{\Psi_{123}^{B_{10}}|f_{1+}^{a_1}f_{1-}^{a_2}f_{2+}^{a_3}\rangle + \Psi_{213}^{B_{10}}|f_{1-}^{a_1}f_{1+}^{a_2}f_{2+}^{a_3}\rangle
$$
$$
+ \Psi_{132}^{B_{10}}|f_{1+}^{a_1}f_{1+}^{a_2}f_{2-}^{a_3}\rangle\},
\tag{17}
$$

and now the scalar functions are

$$
\Psi_{123}^{B_{10}}(x,\boldsymbol{k}_\perp) = \frac{f_{B_{10}}(\mu_F)}{24\sqrt{2}}\phi_{123}^{B_{10}}(x,\mu_F)\Omega_{B_{10}}(x,\boldsymbol{k}_\perp).
\tag{18}
$$

Table 1. The expansion coefficients of the distribution amplitudes $\phi_{123}^{B_{10}}$ of the octet baryons considered in the χ_J decay. The parameters associated with this set of coefficients are $f_{B_{10}}(\mu_0) = 0.0143\,\mathrm{GeV}^2$ and $a_{B_{10}} = 0.80\,\mathrm{GeV}^{-1}$

	B_1	B_2	B_3	B_4	B_5
Δ	0.000	0.000	0.000	0.000	0.000
Σ^*	-0.547	0.182	-0.216	-1.081	0.062
Ξ^*	0.540	-0.180	-0.382	1.742	-0.413

As shown in [11], using the assumption that the nucleon and the delta have the same valence Fock state probabilities, the decuplet decay constant and the transverse size parameter can take a range of values. We take as representative values $f_{B_{10}}(\mu_0) = 0.0143\,\mathrm{GeV}^2$ and $a_{B_{10}} = 0.80\,\mathrm{GeV}^{-1}$.

5 χ_j decay
in the modified hard scattering approach

Since the χ_0 decay into a baryon–antibaryon pair is forbidden by angular momentum conservation and the not-yet-confirmed $^1P_1$ state h_c cannot preserve C-parity and parity simultaneously in this decay mode [22] in a perturbative approach, only χ_1 and χ_2 may have finite partial decay widths[1] into a baryon–antibaryon pair. The helicity amplitudes in covariant form in terms of the baryon–antibaryon spinors $u_B(p,\lambda)$ and $v_B(p,\lambda)$ suitable for our consideration are, for χ_1

$$\mathcal{M}_{\lambda_1\lambda_2\lambda}^1 = \bar{u}_B(p_1,\lambda_1)\mathcal{B}_1\gamma^\nu v_B(p_2,\lambda_2)\epsilon_\nu(\lambda), \qquad (19)$$

and for χ_2

$$\mathcal{M}_{\lambda_1\lambda_2\lambda}^2 = \bar{u}_B(p_1,\lambda_1)\mathcal{B}_2\gamma^\nu v_B(p_2,\lambda_2)\epsilon_{\mu\nu}(\lambda) \\ \times \frac{(p_2^\mu - p_1^\mu)}{M_{\chi_2}}, \qquad (20)$$

where ϵ_μ and $\epsilon_{\mu\nu}$ are the polarization vector and tensor of χ_1 and χ_2, respectively and $\mathcal{B}_J$ are their corresponding decay form factors. Note that (19) and (20) are the only covariant forms permitted for the corresponding helicity amplitudes. Using only γ^μ, $(p_2 - p_1)^\mu$ and $g^{\mu\nu}$ to form a vector and a symmetric tensor, they are the only form that can be constructed which still respects helicity conservation. The decay widths into a baryon–antibaryon are therefore

$$\Gamma(\chi_1 \to B\bar{B}) = \frac{\rho_{\mathrm{p.s.}}(M_B/M_{\chi_1})}{16\pi M_{\chi_1}}\frac{1}{3}\sum_{\lambda's}\left|\mathcal{M}_{\lambda_1\lambda_2\lambda}^1\right|^2$$

---

[1] In practice, χ_0 has a surprisingly large upper bound on the partial width of the decay channel in question [23] and the h_c may also have a non-zero partial decay width. This should be attributed to non-perturbative soft physics or higher twist effects since mass corrections alone should not yield such a large width assuming that the experimental width is near the upper limit

$$= \frac{\rho_{\mathrm{p.s.}}(M_B/M_{\chi_1})m_c^2}{3\pi M_{\chi_1}}\left|\mathcal{B}_1^B\right|^2, \qquad (21)$$

and

$$\Gamma(\chi_2 \to B\bar{B}) = \frac{\rho_{\mathrm{p.s.}}(M_B/M_{\chi_2})}{16\pi M_{\chi_2}}\frac{1}{5}\sum_{\lambda's}\left|\mathcal{M}_{\lambda_1\lambda_2\lambda}^2\right|^2$$

$$= \frac{\rho_{\mathrm{p.s.}}(M_B/M_{\chi_2})m_c^2}{10\pi M_{\chi_2}}\left|\mathcal{B}_2^B\right|^2. \qquad (22)$$

Since in the standard or modified hard scattering scheme baryons are treated as massless in comparison to the large scale M of the process, phase space must be corrected. This is taken care of by the phase space factor in the above equations given by $\rho_{\mathrm{p.s.}}(z) = (1 - 4z^2)^{1/2}$.

Within the SHSA, one has a factorization by which the soft infrared physics is contained in the light-cone wave functions and a perturbatively calculable hard scattering amplitude T_H. In the present problem, the hard scale is set by twice the charm quark mass $2m_c$, rather than by the charmonium mass M_{χ_J}, because, as we mentioned before, the $c\bar{c}$ pair annihilates at a much smaller size than that of the charmonium. This explains the appearance of m_c^2 in (21) and (22). The decay amplitudes, or equivalently, the decay form factors $\mathcal{B}^J$ are expressed as a convolution of the hadron wave functions and the hard scattering amplitude T_H. Based on this approach, there are already a number of works on charmonium decay into the nucleon–antinucleon [24–27]. However, we consider these as incomplete for the following reasons. First, they used a number of nucleon wave functions which did not describe the correct physics at the scale of the order of M_{χ_J}. As shown in [8], none of these wave functions are able to describe the data of the nucleon magnetic form factor. Second, their treatments of α_s are ambiguous given that the decay widths depend on α_s^6; any small changes in the value of α_s used will change the width considerably. It is therefore not difficult to obtain a width that matches the experimental decay widths. All one has to do is to choose the right value of α_s. This is very arbitrary in our opinion. A better way is to determine the scale at which α_s should be evaluated by using the virtualities of the internal exchanged gluons. However, these virtualities in the SHSA depend on the light-cone momentum fractions. One will encounter problems as the end point region is approached when some of these gluon virtualities drop down to Λ_{QCD}^2. α_s will become large and the perturbative part of the SHSA breaks down. another treatment of this problem such as arbitrarily freezing α_s at some values as the virtualities become small, or using an equally arbitrary gluon mass, is not well justified. Third, as we have already discussed due to the development first shown in [3,4] that the contributions from the next higher Fock state of the P-wave charmonium, where the $c\bar{c}$ pair is in a color octet, are comparable to that of the lowest color singlet contribution because of the suppression by angular momentum. To the best of our knowledge, color octet contributions have not been taken into account in most exclusive reaction involving P- and higher wave charmonium. In the case of the decay into light pseudoscalar mesons,

this has been worked out recently within the SHSA in [20] and within the MHSA in [21].

To deal with the above deficiencies of the previous calculations, the phenomenologically constructed nucleon wave function and its generalization to the whole of the octet and decuplet baryon multiplets [10,11] should provide better baryon wave functions at around $10\,\mathrm{GeV}^2$. The problem with the coupling can be dealt with successfully with the MHSA, although it complicates the calculation with the additional, but necessary transverse momentum dependence for a self-consistent description. The above mentioned end point problem in which one runs into the infrared non-perturbative region within a perturbative scheme is cured by the introduction of radiative corrections in the form of a Sudakov factor which spans the energy range between the lower factorization scale μ_F and the higher hard scale of the process in question. The Sudakov factor with transverse size dependence was first calculated in [12,13] and was shown to cure the problem in the case of the pseudoscalar meson scattering. In the case of baryons, this will provide a cure of the above problem only if one supplements the Sudakov suppression factor with the MAX prescription for deciding the infrared cutoff scale [8]. This amounts to choosing the largest transverse separation scale as the infrared cutoff, which is physical in the sense that very long wavelength gluons cannot resolve a "small" hadron which is a color singlet as far as the gluon is concerned.

6 Color singlet contribution

P-wave charmonium decays dominantly through annihilation into gluons, which is a short distance process set by the scale of the charmonium mass M_{χ_J}. The nonperturbative information of the bounded system must come from and be parametrized by the wave function of the χ_J at a small spatial separation, usually taken to be at the origin. For P-wave charmonium, the vanishing of the wave function at the origin forces the substitution of the wave function there by the first derivative of the radial wave function

$$R_P'(0) = \frac{4\mathrm{i}\sqrt{\pi m_c}}{3\sqrt{3}} \int \frac{\mathrm{d}^3\boldsymbol{k}\,\boldsymbol{k}^2}{(2\pi)^3 2M_{\chi_{J=1,2}}} \tilde{\Psi}^{(1)}_{J=1,2}(k)$$
$$= \mathrm{i}\sqrt{\frac{16\pi m_c}{3}} f^{(1)}_{\chi_{J=1,2}}, \tag{23}$$

where $|R_P'(0)| = 0.22\,\mathrm{GeV}^{5/2}$ and $\Psi^{(1)}_{J=1,2}(k)$ are functions of the internal relative momentum of the $c\bar{c}$ system and are the reduced wave functions of the χ_J; that means a power of k has been extracted and put into the covariant spin part of the χ_J wave functions. This is the form of the wave function commonly used for χ_J. The related but more general form of the color singlet wave functions of the χ_J for $J = 1, 2$ are

$$|\chi_1^{(1)}, p\rangle = \frac{\delta_{ab}}{\sqrt{3}} \int \frac{\mathrm{d}^3\boldsymbol{k}}{(2\pi)^3 2M_{\chi_1}} \tilde{\Psi}_1^{(1)}(k)$$

$$\times S_1^{(1)}(p,k)|c\bar{c}; k, p\rangle, \tag{24}$$

$$|\chi_2^{(1)}, p\rangle = \frac{\delta_{ab}}{\sqrt{3}} \int \frac{\mathrm{d}^3\boldsymbol{k}}{(2\pi)^3 2M_{\chi_2}} \tilde{\Psi}_2^{(1)}(k)$$
$$\times S_2^{(1)}(p,k)|c\bar{c}; k, p\rangle, \tag{25}$$

and the covariant spin wave functions of χ_1 and χ_2 expanded up to $O(k^2)$ are

$$S_1^{(1)}(p,k) = \frac{-\mathrm{i}}{2M_{\chi_1}} \left[\slashed{p} + M_{\chi_1} - \frac{2}{M_{\chi_1}} \slashed{p}\slashed{K} \right]$$
$$\times \epsilon_{\mu\nu\alpha\beta} p^\mu \epsilon^\nu K^\alpha \gamma^\beta, \tag{26}$$

$$S_2^{(1)}(p,k) = \frac{1}{\sqrt{2}} [(\slashed{p} + M_{\chi_2})\gamma_\mu$$
$$+ \frac{2}{M_{\chi_2}} [(\slashed{p} + M_{\chi_2})K_\mu - \slashed{p}\slashed{K}\gamma_\mu]] \epsilon^{\mu\nu} K_\nu, \tag{27}$$

where $K \cdot p = 0$. The δ_{ab} in the above equations is to ensure that the $c\bar{c}$ is indeed in a color singlet state.

Since the χ_J are even under charge conjugation, they can annihilate into two or three gluons at leading order $O(\alpha_s^3)$ [28]. The possible types of diagrams for $c\bar{c}$ annihilation into three light quark–antiquark pairs are shown in Fig. 1. As discussed in [28], a color singlet quark–antiquark system has C-parity $(-1)^{L+S}$, so P-wave spin-1 charmonia states are all even C-parity states. Since strong interactions respect C-parity conservation, the intermediate two or three gluons must also be even under charge conjugation. Two gluons in a color singlet state are automatically in an even C-parity state so Figs. 1a,b are possible at the two gluon stage. However in color space, an examination of the color structure of the baryon wave functions (14) and (17) show that exchanges between any two quark lines are symmetric but in Fig. 1b there is an antisymmetric 3-gluon coupling so it is eliminated. For the decay via three gluons in Fig. 1c, it is possible for three gluons to be even under C-parity through a f^{abc} coupling, but again symmetry in color space between the three light quark lines forces the three gluons to couple via d^{abc}, which violates C-parity conservation. We are therefore left only with graphs of type a. These can further be divided into four groups. Each group can be obtained from those shown in Fig. 2 by permutations of the three light quark lines. Since it is usual to treat the heavy $c\bar{c}$ as a non-relativistic system, the heavy quarks share energy and momentum equally, or in other words the distribution amplitude of the charmonium is taken to be a delta function which peaks at one-half. With this assumption, the hard scattering amplitude T_H can be worked out. For P-wave decays, one has to keep the relative momentum K of the $c\bar{c}$ system and expand the hard part around $K = 0$ since only terms quadratic in K survive the $\boldsymbol{k}$ integration.

Taking Fig. 2a as an example, with x_i, y_i the momentum fractions and $\boldsymbol{k}_{\perp i}, \boldsymbol{k}'_{\perp i}$ the internal transverse momenta of the valence quarks in the baryon and antibaryon, respectively, the virtualities of the internal lines are
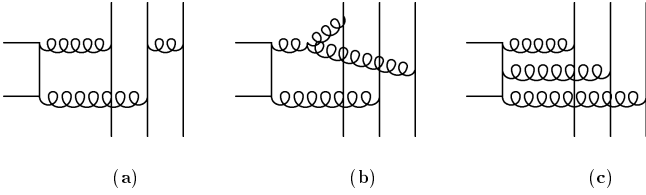
Fig. 1a–c. Basic graphs that could contribute to χ_J color singlet decay. But actually, only graphs of type **a** can contribute
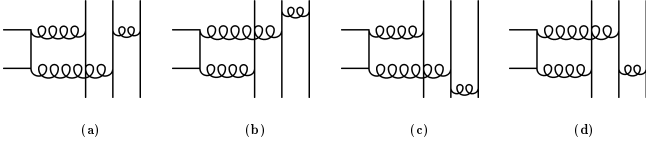

Fig. 2a–d. Graphs of type Fig. 1a can be divided further into four groups

$$
\begin{aligned}
\mathcal{G}_1 &= x_1 y_1 (4m_c^2) - (\boldsymbol{k}_{\perp 1} + \boldsymbol{k}'_{\perp 1})^2 \\
&= \tilde{\mathcal{G}}_1 - (\boldsymbol{k}_{\perp 1} + \boldsymbol{k}'_{\perp 1})^2, \\
\mathcal{G}_2 &= (1 - x_1)(1 - y_1)(4m_c^2) - (\boldsymbol{k}_{\perp 1} + \boldsymbol{k}'_{\perp 1})^2 \\
&= \tilde{\mathcal{G}}_2 - (\boldsymbol{k}_{\perp 1} + \boldsymbol{k}'_{\perp 1})^2, \\
\mathcal{G}_3 &= x_3 y_3 (4m_c^2) - (\boldsymbol{k}_{\perp 3} + \boldsymbol{k}'_{\perp 3})^2 \\
&= \tilde{\mathcal{G}}_3 - (\boldsymbol{k}_{\perp 3} + \boldsymbol{k}'_{\perp 3})^2, \\
\mathcal{Q} &= (1 - x_1) y_3 (4m_c^2) - (\boldsymbol{k}_{\perp 1} - \boldsymbol{k}'_{\perp 3})^2 \\
&= \tilde{\mathcal{Q}} - (\boldsymbol{k}_{\perp 1} - \boldsymbol{k}'_{\perp 3})^2, \\
\mathcal{Q}_c &= 2[x_1(1 - y_1) + y_1(1 - x_1)]m_c^2 \\
&\quad + (\boldsymbol{k}_{\perp 1} + \boldsymbol{k}'_{\perp 1})^2 \\
&= \tilde{\mathcal{Q}}_c + (\boldsymbol{k}_{\perp 1} + \boldsymbol{k}'_{\perp 1})^2.
\end{aligned}
\tag{28}
$$

In fact, Figs. 2a,b give identical contributions and the similar contributions from Figs. 2c,d can be obtained by interchanging x and y. One gets, after sorting and integrating out K, for the hard scattering amplitude

$$
\begin{aligned}
&T_{\mathrm{H}}^J(x, y, \boldsymbol{k}_\perp, \boldsymbol{k}_\perp{}') \\
&= \frac{2^{10}\sqrt{2}(4\pi)^3 m_c^5 \alpha_{\mathrm{s}}(t_1)\alpha_{\mathrm{s}}(t_2)\alpha_{\mathrm{s}}(t_3)}{9\sqrt{3}(\mathcal{G}_1 + \mathrm{i}\epsilon)(\mathcal{G}_2 + \mathrm{i}\epsilon)(\mathcal{G}_3 + \mathrm{i}\epsilon)(\mathcal{Q} + \mathrm{i}\epsilon)(\mathcal{Q}_c - \mathrm{i}\epsilon)} \\
&\quad \times y_3 \left[(1 - 2x_1)^{2-J} + \frac{(-1)^{J-1} 2 m_c^2 x_1 (x_1 - y_1)}{(\mathcal{Q}_c - \mathrm{i}\epsilon)} \right] \\
&\quad + (x \longleftrightarrow y).
\end{aligned}
\tag{29}
$$

To improve perturbation theory via the renormalization group, the square of the renormalization scale μ_R for each running coupling is set to one of the virtualities t_i, $i = 1, 2, 3$, which are chosen by [12,13] as

$$
t_1 = \max(\tilde{\mathcal{G}}_1, \tilde{\mathcal{Q}}_c, 1/b_1^2, 1/b_1'^2),
\tag{30}
$$

$$
t_2 = \max(\tilde{\mathcal{G}}_2, \tilde{\mathcal{Q}}, 1/b_2^2, 1/b_2'^2),
\tag{31}
$$

$$
t_3 = \max(\tilde{\mathcal{G}}_3, 1/b_3^2, 1/b_3'^2),
\tag{32}
$$

with $n_f = 4$ and $\Lambda_{\mathrm{QCD}} = 220\,\mathrm{MeV}$.

These must be convoluted with the wave functions to obtain the color singlet decay form factors. In transverse separation space and in terms of the expressions

$$
\mathcal{C}_1^J(x, y) = y_3(1 - 2x_1)^{2-J},
\tag{33}
$$

$$
\mathcal{C}_2^J(x, y) = (-1)^{J-1} y_3 x_1 (x_1 - y_1),
\tag{34}
$$

the hard scattering part $\hat{T}_{\mathrm{H}}^J$ is

$$
\begin{aligned}
&\hat{T}_{\mathrm{H}}^J(x, y, \boldsymbol{b}, \boldsymbol{b}') \\
&= \frac{2^9 \sqrt{2} m_c}{9\sqrt{3}} \alpha_{\mathrm{s}}(t_1)\alpha_{\mathrm{s}}(t_2)\alpha_{\mathrm{s}}(t_3) \delta^2(\boldsymbol{b}_1 - \boldsymbol{b}_1' - \boldsymbol{b}_3 + \boldsymbol{b}_3') \\
&\quad \times \frac{\mathrm{i}\pi}{2} H_0^{(1)}(\sqrt{x_3 y_3}(2m_c)|\boldsymbol{b}_3|) \\
&\quad \times \frac{\mathrm{i}\pi}{2} H_0^{(1)}(\sqrt{(1 - x_1)y_3}(2m_c)|\boldsymbol{b}_1 - \boldsymbol{b}_1'|) \\
&\quad \times \Bigg\{ \mathrm{i}\pi \Bigg[\frac{H_0^{(1)}(\sqrt{x_1 y_1}(2m_c)|\boldsymbol{b}_1'|)}{(x_1 + y + 1)(1 - x_1 - y_1)} \\
&\quad \times \left(\mathcal{C}_1^J(x, y) + \frac{\mathcal{C}_2^J(x, y)}{x_1 + y_1} \right) \\
&\quad - \frac{H_0^{(1)}(\sqrt{(1 - x_1)(1 - y_1)}(2m_c)|\boldsymbol{b}_1'|)}{(1 - x_1 - y_1)(2 - x_1 - y_1)} \\
&\quad \times \left(\mathcal{C}_1^J(x, y) + \frac{\mathcal{C}_2^J(x, y)}{2 - x_1 - y_1} \right) \Bigg] \\
&\quad - \frac{4}{\pi} \frac{K_0^{(1)}(\sqrt{x_1(1 - y_1) + y_1(1 - x_1)} m_c |\boldsymbol{b}_1'|)}{(x_1 + y_1)(2 - x_1 - y_1)} \\
&\quad \times \left(\mathcal{C}_1^J(x, y) + \frac{2\mathcal{C}_2^J(x, y)}{(x_1 + y_1)(2 - x_1 - y_1)} \right) \\
&\quad - \frac{2 m_c |\boldsymbol{b}_1'| \mathcal{C}_2^J(x, y)}{\sqrt{x_1(1 - y_1) + y_1(1 - x_1)}} \\
&\quad \times \frac{K_1^{(1)}(\sqrt{x_1(1 - y_1) + y_1(1 - x_1)} m_c |\boldsymbol{b}_1'|)}{(2 - x_1 - y_1)(x_1 + y_1)} \Bigg\} \\
&\quad + ((x, \boldsymbol{b}) \longleftrightarrow (y, \boldsymbol{b}')).
\end{aligned}
\tag{35}
$$

With this, the decay form factor can be expressed as

$$
\begin{aligned}
\mathcal{B}_J^{B(1)} &= -\mathrm{i} \frac{\sqrt{3}|R_p'(0)|\sigma_J}{8\sqrt{\pi} m_c^{3/2}} \\
&\quad \times \int [\mathrm{d}x][\mathrm{d}y] \frac{\mathrm{d}^2 \boldsymbol{b}_1}{(4\pi)} \frac{\mathrm{d}^2 \boldsymbol{b}_3}{(4\pi)} \frac{\mathrm{d}^2 \boldsymbol{b}_1'}{(4\pi)} \frac{\mathrm{d}^2 \boldsymbol{b}_3'}{(4\pi)} \\
&\quad \times \hat{T}_{\mathrm{H}}^J(x, y, \boldsymbol{b}, \boldsymbol{b}') \exp[-S(x, y, \boldsymbol{b}, \boldsymbol{b}', 2m_c)] \\
&\quad \times \|\hat{\Psi}^B(x, \boldsymbol{b}) \hat{\Psi}^B(y, \boldsymbol{b}')\|,
\end{aligned}
\tag{36}
$$

where $\sigma_J = 1/(2)^{1/2}, 1$ for $J = 1, 2$, respectively, and the Sudakov correction factor evaluated at the scale of $2m_c$ is included in the convolution. As mentioned earlier, the presence of this radiative correction in the intermediate scale range, together with the MAX prescription for the infrared cut-off in the Sudakov factor, $\tilde{b} = \max(b_1, b_2, b_3, b_1', b_2', b_3')$, renders the whole approach self-consistent. Actually, since there are two hadrons in the final state, one can have a separate infrared scale for each hadron, for example $\tilde{b} = \max(b_1, b_2, b_3)$ and $\tilde{b}' = \max(b_1', b_2', b_3')$. However, numerically this would make no difference so we merge the two into one scale. The factorization

Table 2. Clearly, the color singlet contributions are insufficient for explaining the experimental data of χ_J decay into $p\bar{p}$

J	$\Gamma^{(1)}(\chi_J \to p\bar{p})$ (eV)	PDG (eV) [23]	BES (eV) [29]
1	2.53	75.68	37.84
2	16.58	200.00	118.00

scale μ_F in the wave function is then set to $\mu_F = 1/\tilde{b}$ as usual.

The spin structure of the contribution from the diagrams of Fig. 2 requires J_z of the charmonium to be equal to S_z of the quark line that is not attached to other light quark lines via a gluon, i.e. the first quark line from the left of the three vertical lines in any of the figures in Fig. 2. This permits two possibilities for the helicities, that is $(+, +, -)$ and $(+, -, +)$ of the u- and d-quark lines in Fig. 2 from left to right. The hard scattering amplitudes are, however, identical for the two arrangements of helicities. This gives the following sums of products of the Fourier transform of the scalar functions Ψ^B_{123} of the baryon–antibaryon, given in (6) and (18), represented in (36) by $\|\hat{\Psi}^B(x, \boldsymbol{b})\hat{\Psi}^B(y, \boldsymbol{b}')\|$. We have

$$
\begin{aligned}
&\|\hat{\Psi}^{B_8}(x, \boldsymbol{b})\hat{\Psi}^{B_8}(y, \boldsymbol{b}')\| \\
&= 2\{\hat{\Psi}^{B_8}_{123}(x, \boldsymbol{b})\hat{\Psi}^{B_8}_{123}(y, \boldsymbol{b}') + \hat{\Psi}^{B_8}_{321}(x, \boldsymbol{b})\hat{\Psi}^{B_8}_{321}(y, \boldsymbol{b}') \\
&+ (\hat{\Psi}^{B_8}_{123}(x, \boldsymbol{b}) + \hat{\Psi}^{B_8}_{321}(x, \boldsymbol{b}))(\hat{\Psi}^{B_8}_{123}(y, \boldsymbol{b}') + \hat{\Psi}^{B_8}_{321}(y, \boldsymbol{b}')) \\
&+ (2 \longleftrightarrow 3)\},
\end{aligned} \tag{37}
$$

$$
\begin{aligned}
&\|\hat{\Psi}^{\Lambda}(x, \boldsymbol{b})\hat{\Psi}^{\Lambda}(y, \boldsymbol{b}')\| \\
&= 6\{\hat{\Psi}^{\Lambda}_{123}(x, \boldsymbol{b})\hat{\Psi}^{\Lambda}_{123}(y, \boldsymbol{b}') + \hat{\Psi}^{\Lambda}_{321}(x, \boldsymbol{b})\hat{\Psi}^{\Lambda}_{321}(y, \boldsymbol{b}') \\
&+ (\hat{\Psi}^{\Lambda}_{123}(x, \boldsymbol{b}) - \hat{\Psi}^{\Lambda}_{321}(x, \boldsymbol{b}))(\hat{\Psi}^{\Lambda}_{123}(y, \boldsymbol{b}') - \hat{\Psi}^{\Lambda}_{321}(y, \boldsymbol{b}')) \\
&+ (2 \longleftrightarrow 3)\},
\end{aligned} \tag{38}
$$

$$
\begin{aligned}
&\|\hat{\Psi}^{B_{10}}(x, \boldsymbol{b})\hat{\Psi}^{B_{10}}(y, \boldsymbol{b}')\| \\
&= 3\{\hat{\Psi}^{B_{10}}_{123}(x, \boldsymbol{b})\hat{\Psi}^{B_{10}}_{123}(y, \boldsymbol{b}') + \hat{\Psi}^{B_{10}}_{321}(x, \boldsymbol{b})\hat{\Psi}^{B_{10}}_{321}(y, \boldsymbol{b}') \\
&+ \hat{\Psi}^{B_{10}}_{132}(x, \boldsymbol{b})\hat{\Psi}^{B_{10}}_{132}(y, \boldsymbol{b}') + \hat{\Psi}^{B_{10}}_{231}(x, \boldsymbol{b})\hat{\Psi}^{B_{10}}_{231}(y, \boldsymbol{b}')\}.
\end{aligned} \tag{39}
$$

The results for the color singlet contributions in χ_1 and χ_2 decay into a nucleon–antinucleon pair are shown in Table 2[2] together with the experimental measurements. It is clear that the singlet contribution is insufficient even with the smaller results of the BES collaboration [29] to account for the experimental measurements. For uncertainties in the theoretical estimate of the color singlet contribution, the consistence of this calculation within MHSA, the choice of the proton wave function and the value of the proton decay constant used etc., we refer to [14]. We will further discuss the differences between the experimental results in a later section. The very important color octet contribution will be investigated in the following section.

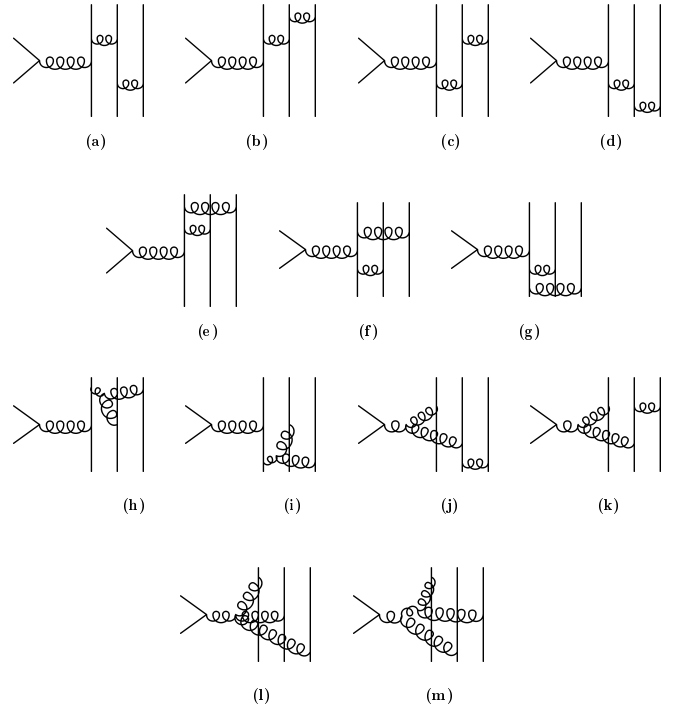[2] Our present numbers supersede those previously reported in [30]

Fig. 3a–m. In addition to the graphs of type Fig. 1, these form the bases of further contributions in the color octet decay channel

7 Color octet contribution

In color octet $c\bar{c}$ decays into a baryon–antibaryon system, there is a constituent gluon in the initial state so the C-parity arguments given in Sect. 6 no longer hold. The diagrams in Fig. 1 then form the bases of three different contributing groups. The other possibilities are from the graphs where the $c\bar{c}$ pair annihilates into a single gluon, which would not be possible if the pair were in a color singlet state. These additional groups are shown in Fig. 3.

In order to form a color singlet baryon–antibaryon in the final states, this net color from the constituent gluon must be neutralized. One could allow it to enter directly into one of the final baryons as a constituent of a higher Fock state of the latter. However, within the hard scattering approach, at least one hard gluon must be exchanged between all the constituent partons; therefore such a contribution involving the next higher Fock state of the baryons will be suppressed by the hard scale of the process and also by the smaller probability of the next Fock state. In any case, bringing in a higher state unnecessarily will introduce additional unknown wave functions. It is therefore best to avoid it. The introduction of the color octet in the charmonium system is, on the contrary, well founded and is indeed necessary as shown in [3, 4] and as we argued earlier. The alternative for color neutralization is done by attaching the constituent gluon onto all possible places in the diagrams of Fig. 1, Figs. 2 and 3. This will generate about 9–11 diagrams for each group and the light quark lines will also have to be permuted and so altogether there are over two hundred diagrams. For-

tunately, the tedious algebra can be handled completely by the computer program FORM, and one can arrange the constituent gluon to be attached automatically to all possible places in each basic graph and work out the color factors as well as the perturbative hard scattering part entirely by using this program. In fact, none of the algebra needs to be worked out by hand.

The color octet wave function of the charmonium is

$$|\chi_{\chi_J}^{(8)}, p\rangle = \frac{t_{c\bar{c}}^a}{2} f_{\chi_J}^{(8)} \int [\mathrm{d}z] \phi_{\chi_J}^{(8)}(z_1, z_2, z_3)$$
$$\times S_{J\nu}^{(8)}(p)|c\bar{c}g; p\rangle. \qquad (40)$$

As explained in [11], the distribution amplitudes of the octet charmonium $\phi_{\chi_J}^{(8)}$ are conveniently taken to be delta functions that peak at the light-cone momentum $z_3 = z = 0.15$ for the constituent gluon and $z_1 = z_2 = (1-z)/2$ for the heavy quarks while the octet decay constant $f_{\chi_J}^{(8)}$ are obtained from fits in [20,21]. The covariant spin wave functions for the octet states are given in [21]:

$$S_{1\rho}^{(8)}(p) = \frac{-\mathrm{i}}{2M_{\chi_1}}(\not{p} + M_{\chi_1})\epsilon_{\mu\nu\rho\sigma}p^\mu\epsilon^\nu\gamma^\sigma, \qquad (41)$$

$$S_{2\rho}^{(8)}(p) = \frac{1}{\sqrt{2}}(\not{p} + M_{\chi_2})\epsilon_{\sigma\rho}\gamma^\sigma. \qquad (42)$$

As we will take the spin of the charmonium to be pointing upward without loss of generality, we found it more straightforward to write these as

$$S_{1\rho}^{(8)(+)}(p) = \frac{1}{2}(\not{p} + M_{\chi_1})(\not{\epsilon}_{c\bar{c}}^{(+)}\epsilon_\rho^{(0)} - \not{\epsilon}_{c\bar{c}}^{(0)}\epsilon_\rho^{(+)}), \quad (43)$$

$$S_{2\rho}^{(8)(+)}(p) = \frac{1}{2}(\not{p} + M_{\chi_2})(\not{\epsilon}_{c\bar{c}}^{(+)}\epsilon_\rho^{(0)} + \not{\epsilon}_{c\bar{c}}^{(0)}\epsilon_\rho^{(+)}) \quad (44)$$

instead. The ϵ_ρ is the polarization vector of the constituent gluon and $\epsilon_{c\bar{c}}^\mu$ is the spin $S = 1$ vector of the color octet $c\bar{c}$ system. Then the numerator of any contributing graphs to χ_J decay can all be expressed in the form

$$N^J = \mathcal{A} + (-1)^J \mathcal{A}', \qquad (45)$$

and the difference in the numerator between the χ_1 and χ_2 system comes entirely from the sign. In the Appendix where we list all the contributions from the graphs of each group, the numerators are all in the above format.

To deal with the color octet contributions, bearing in mind the advantages of the dynamical setting of the renormalization scales and the built-in Sudakov suppression of the regions of the distribution amplitudes which are problematic at the end points, one could use again the modified hard scattering scheme [12,13] as we did in the singlet contribution in the previous section. However, these advantages are obtained at the expense of complicating the expressions and the calculations of the perturbative hard part $T_\mathrm{H}(x, \boldsymbol{k}_\perp)$ by including the internal transverse momenta in the propagators. These transverse momenta will have to be integrated out subsequently by convoluting with the hadronic wave functions. Therefore, the number of integration variables can be quite high, especially when

we are dealing with a baryon and an antibaryon which contain three constituent quarks and antiquarks even at the valence level and there are also many diagrams to consider. To keep things simple, it is advisable to return to the standard scheme [1] so as to deal only with the distribution amplitudes and $T_\mathrm{H}(x)$ without the internal transverse momenta, and not the more complicated wave functions and $T_\mathrm{H}(x, \boldsymbol{k}_\perp)$. This is what we will do below. We will discuss how to get the graphs and the expressions for the individual color octet contribution to the amplitude in the next section within the standard scheme.

8 Getting the graphs and calculating T_H of the color octet contributions

In the appendices, we give the graphs and expressions of our calculation for the color octet contribution. The diagrams can be divided into ten basic groups. Each group is based on one basic graph in which the constituent gluon from the color octet component of the charmonium has not yet been drawn out or inserted. Because of the restriction of the C-parity, in the absence of the constituent gluon, these groups individually may or may not exist in the color singlet contribution to the decay. In the latter case, they survive solely because of the presence of the constituent gluon. These graphs are those already presented in Figs. 1 and 3. The group associated with each basic graph is generated by attaching the constituent gluon to all possible places on the basic graph except on the initial c-quark or $\bar{c}$-quark when they have just emerged from the charmonium.

The numerator of the hard part T_H of each diagram from each group will be given in the appendices, while the denominator, which is essentially a product of the propagators in each diagram, will not be written out explicitly individually but can be derived from those of the basic graphs (these will be presented with each group) by following some simple rules that follow from the momentum flow through the graph.

Given that the momenta of the χ_J, and those of the outgoing baryon and antibaryon are P_{χ_J}, P_B and $P_{\bar{B}}$, respectively, the outgoing momenta of the constituents of the baryon and antibaryon will be assigned the momenta $p_{q_i} = x_i P_B$, $p_{\bar{q}_i} = y_i P_{\bar{B}}$ with $i = 1, 2, 3$. Here x_i and y_i are the momentum fraction of the ith light quark line of the outgoing baryon–antibaryon subjected to $\sum_i x_i = \sum_i y_i = 1$. In the basic graphs, the constituent gluon is not included, so the momentum of χ_J shared by the charm–anticharm is $p_c = z_1 P_{\chi_J}$ and $p_{\bar{c}} = z_2 P_{\chi_J}$ with $z_1 + z_2 = 1$. Obviously energy-momentum conservation requires $P_{\chi_J} = P_B + P_{\bar{B}}$. The product of the gluon propagators in each of the basic graphs is expressed with these momentum configurations with $2P_B \cdot P_{\bar{B}} = (2m_c)^2 \gg P_B^2, P_{\bar{B}}^2 \sim 0$. On the insertion of the constituent gluon with momentum fraction z, the condition $z_1 + z_2 = 1$ is now replaced by $z + z_1 + z_2 = 1$. Therefore, the heavy quark pair will have only $(1 - z)P_{\chi_J}$ instead of the full P_{χ_J} to annihilate into gluons. The consequence is that in the new
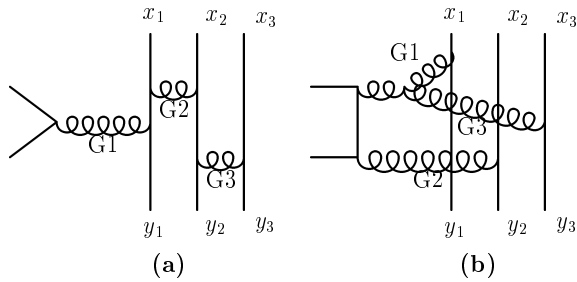
Fig. 4a,b. Our labelling scheme as applied to **a** Group 2 and **b** Group 4

graphs the momenta flowing along the path or lines connecting the initial heavy quark line of the charmonium to the insertion point of the constituent gluon must be reduced by zP_{χ_J}. The momenta in any intermediate heavy quark line(s) which only exist in those graphs where the $c\bar{c}$ annihilates into two or more gluons, may also need to be so adjusted, but that depends on the insertion point. This momentum shift in the basic graphs brings about a similar shift in the momenta carried by the propagators along the same connecting path. In general, this shift can be done by replacing one of the three (x_i, y_i) pairs in the affected propagators including the intermediate heavy quark one by $(x_i - z, y_i - z)$.

The momentum fractions and the quark and gluon lines are labelled as follows for a simpler description, and they apply to all basic graphs. The top (bottom) heavy quark line on the left is the initial charm (anticharm) quark line. The three vertical light quark lines running from the bottom to the top are light quark line 1 to 3 from left to right. Light quarks (antiquarks) of the baryon (antibaryon) emerge from the top (bottom). The fractions x_i and y_i label that of the quark and antiquark of the ith light quark line. The gluon line coming directly or indirectly from the charmonium and entering the ith light quark line is gluon line i, Gi. Whereas the labelling of the vertical light quark line is for the entire line, each of these gluon lines connects only two vertices and ends at these vertices. There will be only one gluon line entering each light quark line even though each light quark line may be attached to more than one gluon line. In this case, only one such line enters the quark line and the other is leaving it. The gluon line is then labelled with Gi if it is entering light quark line i and not leaving it as we mentioned above. Figure 4 illustrates our labelling scheme with some examples. There are, however, gluon lines that enter a 3- or 4-gluon vertex instead of a light quark line, see Group 4 and 6 for examples. These are not labelled. The labelling is for the purpose of identifying the graphs created from the basic one by the insertion of the constituent gluon. The insertion point (I.P.) of the constituent gluon will uniquely identify each graph thus created, and these graphs will form a group based on the basic one. Taking the χ_1 and χ_2 to be spinning up, the allowed helicities of the three light quark lines $(\lambda_1, \lambda_2, \lambda_3)$ are $(+, +, -)$, $(+, -, +)$ and $(-, +, +)$. These three helicity configurations of each graph do not necessarily have the same or a permutation related nu-

merator as in the color singlet case. The presence of the constituent gluon makes this impossible in general. The corresponding numerators are listed in the tables in the appendices.

As mentioned above, each graph created from a basic graph by adding the constituent gluon is identified by the insertion point where the gluon from the color octet state of the charmonium joins the basic graph. The group of a basic graph is created by attaching the color octet gluon to all possible places on the basic graph with the exception of the initial heavy quark or antiquark line. Also the creation of a graph with an intermediate state with one gluon and nothing else is forbidden by C-parity. More explicitly this means that when the basic graph contains the $c\bar{c}$ annihilation into one single gluon, the graph with the constituent gluon attached to this gluon is not possible. Note that this kind of basic graphs by themselves cannot exist without the constituent gluon because of C-parity and so they do not contribute to the color singlet contribution.

The complete graphs created from the basic ones will be labelled as follows. If the constituent gluon attaches to one of the light quark lines, it can be with one of the three quarks (antiquarks) that forms the baryon (antibaryon). These graphs are labelled as Ui or Li indicating that the constituent gluon joins the upper (top) or lower (bottom) part of the quark line i. If the quark line has one or more intermediate off-shell middle segments, which are separated from the upper and lower part by a quark–gluon–antiquark vertex or vertices to which the octet gluon attaches itself, these are labelled Mi for one intermediate off-shell quark line on quark line i, for example the quark line 2 of Group 1 (see Fig. 7), and UMi or LMi denote the upper or lower part of the middle off-shell line if two intermediate middle segments exist on the light quark line i, for example the quark line 1 of Group 8 (see Fig. 15). Evidently, the constituent gluon can be attached to the gluon lines as well. These graphs are labelled with Gi (not to be confused with the gluon line labelling) if the new graph is created by joining the gluon to the gluon line i by a 3-gluon vertex. If the gluon is attached instead to an unlabelled gluon line, the graph will be called GR as the constituent gluon attaches to the remaining unlabelled gluon line. Only one such graph per group is possible at maximum and these always vanish due to color. We will not discuss these graphs further. Whenever a 3-gluon vertex exists in a basic graph, there is the possibility of attaching the constituent gluon to this vertex to create a complete graph with a 4-gluon vertex. These will be labelled as 4G for one such possibility or 4G1 and 4G2 when two such possibilities exist as in Group 9 (see Fig. 16). There remains attaching the gluon to the heavy intermediate heavy quark line(s) when this exists. We denote this simply by graph Q for only one heavy quark line or UQ and LQ in the presence of two heavy quark lines, one situated above the other on the basic graph, meaning the gluon is attached to the upper or lower heavy quark line. The latter is possible only for Group 5.

The rules for getting the product of propagators for each new graph from that of the basic graphs are as fol-

lows. In determining which of the pair (x_i, y_i) in the propagators to replace by $(x_i - z, y_i - z)$, it is the i pair for graphs labelled Ui, Li, Gi, Mi, UMi or LMi. The replacement should only be made to propagators along the line connecting the heavy quark line to the insertion point whether they contain (x_i, y_i) explicitly or not. A modification must be made to gluon or light quark propagators through the relation $x_i = 1 - x_j - x_k$ and $y_i = 1 - y_j - y_k$ where $j \neq k \neq i$ and also to any charm propagator only if it contains the pair (x_i, y_i) explicitly. So applying this to graph U1 of Group 5 illustrated in Fig. 5a, only the propagators associated with the gluon line G1 and the upper heavy quark line in Fig. 12 need this replacement. The product becomes

$$\frac{1}{\{(z_1 + z - x_1)(z_1 + z - y_1) - 1/4\}(2m_c)^2}$$
$$\times \frac{1}{\{(z_2 - x_3)(z_2 - y_3) - 1/4\}(2m_c)^2} \tag{46}$$
$$\times \frac{1}{(x_1 - z)(y_1 - z)(2m_c)^2 + \rho^2} \frac{1}{x_2 y_2 (2m_c)^2} \frac{1}{x_3 y_3 (2m_c)^2}.$$

If it is graph L2 of Group 5 in Fig. 5b, only the propagator of gluon line G2 needs to be changed, and we have

$$\frac{1}{\{(z_1 - x_1)(z_1 - y_1) - 1/4\}(2m_c)^2}$$
$$\times \frac{1}{\{(z_2 - x_3)(z_2 - y_3) - 1/4\}(2m_c)^2} \tag{47}$$
$$\times \frac{1}{x_1 y_1 (2m_c)^2} \frac{1}{(x_2 - z)(y_2 - z)(2m_c)^2 + \rho^2} \frac{1}{x_3 y_3 (2m_c)^2}.$$

As a third example, applying this to Fig. 5c, that is graph L3 of Group 1, gives

$$\frac{1}{(1 - z)^2 (2m_c)^2} \frac{1}{(x_3 - z)(1 - y_1 - z)(2m_c)^2 + \rho^2}$$
$$\times \frac{1}{x_1 y_1 (2m_c)^2} \frac{1}{(1 - x_1 - z)(1 - y_1 - z)(2m_c)^2 + \rho^2}$$
$$\times \frac{1}{(x_3 - z)(y_3 - z)(2m_c)^2 + \rho^2}. \tag{48}$$

It must be mentioned that in the appendices where details of each group are given, the propagators are written down without the usual iϵ. This is to save on typing but it should be understood implicitly that a iϵ should be present in each propagator. This also applies to the expressions here. Also, we have inserted a term ρ^2 in the denominators of those propagators which carry two poles which cannot be handled by the iϵ prescription. The ρ^2 is understood to be the mean squared internal momentum of the baryons $\rho^2 = \langle \boldsymbol{k}_\perp^2 \rangle$. It is used here to prevent two possible poles in any one propagator to occur simultaneously. This problem has been treated in the same manner in [20] whenever the iϵ prescription failed. The actual values of ρ^2 depend on the baryon wave functions. We used $\rho_{(8)} = 415.0$ MeV and $\rho_{(10)} = 389.0$ MeV for the octet and decuplet baryons, respectively. These values are obtained from the respective wave functions.
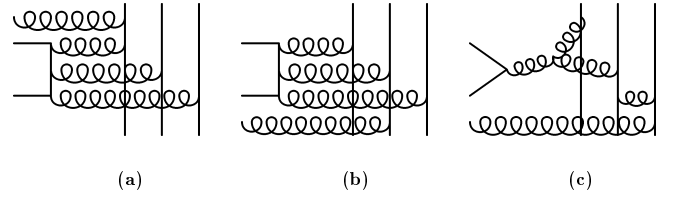

Fig. 5a–c. Examples of complete color octet graphs. **a** graph U1 and **b** graph L2 of Group 5, and **c** graph L3 of Group 1
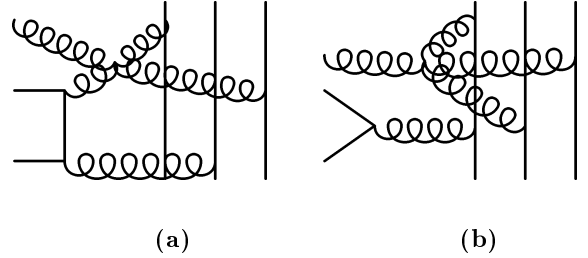

Fig. 6a,b. Examples of complete color octet graphs with 4-gluon vertex. **a** graph 4G of Group 4 and **b** graph 4G of Group 10

For 4G graphs, if the unlabelled gluon line attaches to the 3-gluon vertex connecting gluon line Gi and Gj, then either replace (x_i, y_i) with $(x_i - z, y_i - z)$ or (x_j, y_j) with $(x_j - z, y_j - z)$ in the gluon propagator and do the same in the heavy quark propagator but in this case only when either pair of momentum fractions appears explicitly is sufficient. Applying this to Group 4, we get

$$\frac{1}{\{(z_2 - x_2)(z_2 - y_2) - 1/4\}(2m_c)^2}$$
$$\times \frac{1}{(1 - x_2 - z)(1 - y_2 - z)(2m_c)^2 + \rho^2}$$
$$\times \frac{1}{x_1 y_1 (2m_c)^2} \frac{1}{x_2 y_2 (2m_c)^2} \frac{1}{x_3 y_3 (2m_c)^2}, \tag{49}$$

and to Group 10, the products of the propagator become

$$\frac{1}{(1 - z)^2 (2m_c)^2} \frac{1}{(1 - z)(1 - y_1 - z)(2m_c)^2}$$
$$\times \frac{1}{(1 - x_1 - z)(1 - y_1 - z)(2m_c)^2 + \rho^2}$$
$$\times \frac{1}{x_2 y_2 (2m_c)^2} \frac{1}{x_3 y_3 (2m_c)^2}. \tag{50}$$

Equations (48) and (50) are fine examples of the necessity of having to make the shift even if either pair of the momentum fractions does not appear explicitly in the light quark and gluon propagators. In this example, the replacement has to be made even for $x_1 + x_2 + x_3 = y_1 + y_2 + y_3 = 1$ to $1 - z$ because the momentum fractions are completely hidden. For the remaining Q, UQ and LQ graphs, it is only necessary to replace z_1 by $z_1 + z$, and z_2 must be left alone.

One must not forget that the insertion of the constituent gluon will introduce an additional propagator (X-Prop.) to the basic graph. This is, however, not true for

the 4G graphs but these have a factor $(2m_c)^2$ less than the other graphs and so a factor of $1/(2m_c)^2$ must be multiplied to them so that a global prefactor can be written down for all graphs. The extra propagator or the extra factor $1/(2m_c)^2$ is given in the last table of the numerators of each group in the column X-Prop. Similarly, the structure of group 6 is such that it is a factor $(2m_c)^2$ less than the other group from the start because these graphs have one propagator less. In order to keep the same overall factor for all groups, $1/(2m_c)^2$ has been multiplied to the product of the basic propagators of this group. This extra factor of course does not correspond to any propagator but is merely a compensation factor. It must be mentioned that not all graphs generated from the basic graphs exist. Some vanish for one reason or another. For these, the additional propagators are not given in the tables but have the entry n.g. (not given) instead.

There exist several more groups that we have not drawn out explicitly in the appendices. Their basic graphs may be obtained from those of Group 1, 2 and 2', 3, 4, 7 and 10 by making one simple change to them. For example, attaching the line G2 to quark line 1 at a point below instead of above the line G1 on Group 2 and 2', or moving line G3 in Group 1 and 3 to above the $qg\bar{q}$-vertex on quark line 2, or flipping any of the basic graphs of Group 3, 4, 7 and 10 upside down. However, these extra groups may be included by giving a factor of two on each of their associated group because these are related to each other by a simple change of variables. Finally, we must mention that the graphs in each group must be subjected to further permutations of the three light quark lines to give further graphs. But these also can be taken care of by a numerical factor so each possible insertion point will generate only one graph and there is no need to divide the graphs any further or add any more groups.

9 Color singlet and octet contribution in the standard scheme

9.1 Color singlet contribution

The procedure to obtain the color singlet contribution in the standard scheme is quite similar to the one we used in Sect. 6. Remembering that in the standard scheme, the internal transverse momenta are taken to be negligible in comparison with the virtualities in all propagators in the perturbative hard part, $T_{\mathrm{H}}(x)$ is free from any $\boldsymbol{k}_\perp$'s and the latter can be integrated over each wave function to give the corresponding distribution amplitude. So setting the $\boldsymbol{k}_\perp$'s in $\mathcal{G}_i$, $\mathcal{Q}$ and $\mathcal{Q}_c$ in (28) to zero, T_{H}^J is now independent of $\boldsymbol{k}_\perp$ and $\boldsymbol{k}_\perp'$:

$$
\begin{aligned}
T_{\mathrm{H}}^J(x,y) = {} & \frac{2\sqrt{2}(4\pi)^3(\alpha_{\mathrm{s}}(m_c))^3}{9\sqrt{3}m_c^5 x_1 x_3 y_1 y_3 (1-x_1)^2(1-y_1)} \\
& \times \frac{1}{[x_1(1-y_1)+y_1(1-x_1)]} \\
& \times \left[(1-2x_1)^{2-J} + \frac{(-1)^{J-1}x_1(x_1-y_1)}{x_1(1-y_1)+y_1(1-x_1)} \right]
\end{aligned}
$$

$$
+ (x \longleftrightarrow y). \tag{51}
$$

The renormalization scale μ_R in the above equation has been set at the constant scale m_c in α_{s} because each gluon takes approximately $M_{\chi_J}/2 \approx m_c$ from the charmonium and so the virtuality is roughly m_c^2. Now Fourier transforming the transverse-momentum-independent T_{H}^J of transverse position-space yields several delta functions which force all $\boldsymbol{b}$'s and $\boldsymbol{b}'$'s to the origin. As a consequence, as follows from its definition and derivation, the Sudakov factor has to be set to unity. The decay form factor defined in Sect. 5 of χ_J into $B - \bar{B}$ becomes

$$
\begin{aligned}
\mathcal{B}_J^{B(1)} = {} & -\mathrm{i}\frac{\sqrt{3}|R_p'(0)|\sigma_J}{8\sqrt{\pi}m_c^{3/2}(4\pi)^4} \int [\mathrm{d}x][\mathrm{d}y] T_{\mathrm{H}}^{J(1)}(x,y) \\
& \times \|\hat{\Psi}^B(x,0)\hat{\Psi}^B(y,0)\|,
\end{aligned} \tag{52}
$$

where $\sigma_J = 1/(2)^{1/2}, 1$ for $J = 1, 2$ as before. This has to be combined with that of the color octet contribution to be discussed below in accordance with our theoretical arguments given in Sect. 3 to give the true partial decay width.

9.2 Color octet contribution

The total color octet contribution to $\mathcal{B}_J^{B(8)}$ has to be the sum over all contributing graphs from each group and over all possible helicity configurations of the light quarks and antiquarks in the outgoing baryon–antibaryon given in the appendices:

$$
\begin{aligned}
\mathcal{B}_J^{B(8)} = {} & \sum_{\lambda_1,\lambda_2,\lambda_3=\pm} \frac{f_{\chi_J}^{(8)}\sigma_J}{2m_c(4\pi)^4} \\
& \times \int [\mathrm{d}x][\mathrm{d}y]\{T_{\mathrm{H}}^{J(8)}(x,y)\}_{\lambda_1,\lambda_2,\lambda_3} \\
& \times \|\hat{\Psi}^B(x,0)\hat{\Psi}^B(y,0)\|_{\lambda_1,\lambda_2,\lambda_3}.
\end{aligned} \tag{53}
$$

The helicity dependent hard perturbative parts are

$$
\begin{aligned}
& \{T_{\mathrm{H}}^{J(8)}(x,y)\}_{\lambda_1,\lambda_2,\lambda_3} \\
& = i(4\pi\alpha_{\mathrm{s}}(m_c))^3\sqrt{4\pi\alpha_{\mathrm{s}}^{soft}}(2m_c)^7 \\
& \times \sum_{\substack{g\in\mathrm{Groups} \\ m\in\mathrm{Members}}} S_g P_{gm}(x,y)\{N_{gm}^J(x,y)\}_{\lambda_1,\lambda_2,\lambda_3},
\end{aligned} \tag{54}
$$

where $P_{gm}(x,y)$ is the product of propagators of the member $m =$ U1, U2, U3, L1, L2, L3, ... etc. of the group $g = 1, 2, 2', ..., 10$. They can be obtained from the product of the basic propagators of each group as discussed in Sect. 8. The S_g is a symmetry factor for the group g to take care of similar potential groups that are related to g by a simple change of variables. For the groups listed in the appendices, $S_g = \{2,2,2,4,2,1,1,2,1,1,2\}$ for the group $g = 1, 2, 2', 3, ..., 10$, respectively. The coupling $\alpha_{\mathrm{s}}^{\mathrm{soft}}$, taken to be equal to π, is that of attaching the constituent gluon to the basic graphs. It needs special

treatment because of its different nature in comparison to the rest of the α_s's [21]. The $\{N_{gm}(x,y)\}_{\lambda_1,\lambda_2,\lambda_3}$ in the above equation contains the helicity dependence and denotes the numerator of the member m of the group g. These numerators are given in the appendices. Note that the calculation is really only gauge-invariant to order z^2 in the numerator (see [21]) because the $c\bar{c}$ is treated as on-shell; therefore all z^3 or higher terms in the numerator have to be dropped. The remaining helicity dependent products of the scalar functions $\Psi^B_{123}(x,0)$ of the baryon wave functions are given below.

$$\|\hat{\Psi}^{B_8}(x,0)\hat{\Psi}^{B_8}(y,0)\|_{+,+,-}$$
$$= 2\{\hat{\Psi}^{B_8}_{132}(x,0)\hat{\Psi}^{B_8}_{132}(y,0) + \hat{\Psi}^{B_8}_{231}(x,0)\hat{\Psi}^{B_8}_{231}(y,0)$$
$$+(\hat{\Psi}^{B_8}_{132}(x,0) + \hat{\Psi}^{B_8}_{231}(x,0))(\hat{\Psi}^{B_8}_{132}(y,0) + \hat{\Psi}^{B_8}_{231}(y,0))\}, \quad (55)$$

$$\|\hat{\Psi}^{B_8}(x,0)\hat{\Psi}^{B_8}(y,0)\|_{+,-,+}$$
$$= 2\{\hat{\Psi}^{B_8}_{123}(x,0)\hat{\Psi}^{B_8}_{123}(y,0) + \hat{\Psi}^{B_8}_{321}(x,0)\hat{\Psi}^{B_8}_{321}(y,0)$$
$$+(\hat{\Psi}^{B_8}_{123}(x,0) + \hat{\Psi}^{B_8}_{321}(x,0))(\hat{\Psi}^{B_8}_{123}(y,0) + \hat{\Psi}^{B_8}_{321}(y,0))\}, \quad (56)$$

$$\|\hat{\Psi}^{B_8}(x,0)\hat{\Psi}^{B_8}(y,0)\|_{-,+,+}$$
$$= 2\{\hat{\Psi}^{B_8}_{213}(x,0)\hat{\Psi}^{B_8}_{213}(y,0) + \hat{\Psi}^{B_8}_{312}(x,0)\hat{\Psi}^{B_8}_{312}(y,0)$$
$$+(\hat{\Psi}^{B_8}_{213}(x,0) + \hat{\Psi}^{B_8}_{312}(x,0))(\hat{\Psi}^{B_8}_{213}(y,0) + \hat{\Psi}^{B_8}_{312}(y,0))\}, \quad (57)$$

$$\|\hat{\Psi}^{\Lambda}(x,0)\hat{\Psi}^{\Lambda}(y,0)\|_{+,+,-}$$
$$= 6\{\hat{\Psi}^{\Lambda}_{132}(x,0)\hat{\Psi}^{\Lambda}_{132}(y,0) + \hat{\Psi}^{\Lambda}_{231}(x,0)\hat{\Psi}^{\Lambda}_{231}(y,0)$$
$$+(\hat{\Psi}^{\Lambda}_{132}(x,0) - \hat{\Psi}^{\Lambda}_{231}(x,0))(\hat{\Psi}^{\Lambda}_{132}(y,0) - \hat{\Psi}^{\Lambda}_{231}(y,0))\}. \quad (58)$$

The other two helicity arrangements of this quantity for the Λ follow the pattern above for the other octet baryons. For the decuplet baryons, they are

$$\|\hat{\Psi}^{B_{10}}(x,0)\hat{\Psi}^{B_{10}}(y,0)\|_{+,+,-}$$
$$= 3\{\hat{\Psi}^{B_{10}}_{132}(x,0)\hat{\Psi}^{B_{10}}_{132}(y,0) + \hat{\Psi}^{B_{10}}_{231}(x,0)\hat{\Psi}^{B_{10}}_{231}(y,0)\}, \quad (59)$$
$$\|\hat{\Psi}^{B_{10}}(x,0)\hat{\Psi}^{B_{10}}(y,0)\|_{+,-,+}$$
$$= 3\{\hat{\Psi}^{B_{10}}_{123}(x,0)\hat{\Psi}^{B_{10}}_{123}(y,0) + \hat{\Psi}^{B_{10}}_{321}(x,0)\hat{\Psi}^{B_{10}}_{321}(y,0)\}, \quad (60)$$
$$\|\hat{\Psi}^{B_{10}}(x,0)\hat{\Psi}^{B_{10}}(y,0)\|_{-,+,+}$$
$$= 3\{\hat{\Psi}^{B_{10}}_{213}(x,0)\hat{\Psi}^{B_{10}}_{213}(y,0) + \hat{\Psi}^{B_{10}}_{312}(x,0)\hat{\Psi}^{B_{10}}_{312}(y,0)\}. \quad (61)$$

With this notation, the color octet contribution looks rather simple. One only has to sum up all graphs from each and every group and then perform the integrations.

10 The widths of χ_j decay into baryon–antibaryons

With our method, discussed in the previous sections, the color octet contribution which we argued to be necessary in addition to the singlet contribution for getting the correct P-wave χ_J partial decay widths can be included. Before giving the numerical results, it must be mentioned that of all the baryons we considered, only the decay into

Table 3. The partial decay widths for χ_J decay into octet and decuplet baryon–antibaryon pairs. The width of $\chi_1 \longrightarrow N\bar{N}$ in parentheses is to indicate that this value is a fit unlike all partial widths of χ_2 which are predictions. Based on this fit, the rest of the χ_1 widths are also predictions

Octet baryons	$\Gamma^{(1)+(8)}$ (eV) $J=1$	$J=2$	Decuplet baryons	$\Gamma^{(1)+(8)}$ (eV) $J=1$	$J=2$
$\chi_J \to N\bar{N}$	(56.27)	154.19	$\chi_J \to \Delta\bar{\Delta}$	33.49	124.62
$\chi_J \to \Sigma\bar{\Sigma}$	28.42	97.69	$\chi_J \to \Sigma^*\bar{\Sigma}^*$	18.46	71.09
$\chi_J \to \Xi\bar{\Xi}$	21.49	72.62	$\chi_J \to \Xi^*\bar{\Xi}^*$	9.42	41.16
$\chi_J \to \Lambda\bar{\Lambda}$	33.64	69.19			

Table 4. Comparing our results with the measured widths from the PDG [23] data and from the BES collaboration [29]. This branching ratio of χ_1 is a fit

	Branching ratios ($\times 10^{-5}$)		
	$Br^{(1)+(8)}$	PDG	BES
$\chi_1 \to p\bar{p}$	(6.39)	8.60 ± 1.2	$4.30 \pm 2.3 \pm 2.9$
$\chi_2 \to p\bar{p}$	7.71	10.00 ± 1.0	$5.90 \pm 3.1 \pm 3.3$

proton–antiproton is measured so the majority of our results are in fact predictions. Moreover, the most recently reported measured values [29] differ by as much as a factor of two from those in the Particle Data Tables [23]. This is also true in the case of the decay into pseudoscalar mesons as noted already in [21]. Therefore we are content with results that lie somewhere in between these measurements. Until the situation improves, the color octet decay constants fitted in [20,21] cannot be more accurately determined, hence neither can the current results. In any case, part of our goals is to show that explicit calculations do indeed support the theoretical arguments, that is, the color octet contribution in P-wave χ_J decays cannot be neglected in inclusive nor in exclusive processes.

Our results are shown in Table 3 for the octet and decuplet baryons. The numerical parameters used to obtain these results which were given throughout this paper have been collected together again in Appendix B so that interested readers do not have to search through the paper for the values. Only the kinematically plausible decuplet baryons with the lowest masses are considered. In getting these results, we used the color octet decay constant $f^{(8)}_{\chi_2} = 0.9 \times 10^{-3}\,\mathrm{GeV}^2$ fitted in [20] for the decay of $\chi_2 \to \pi\pi$ within the standard hard scattering approach. We found that in order to obtain reasonable agreement of the $\chi_1 \to p\bar{p}$ decay, it must have a smaller color octet decay constant. Therefore, we use $f^{(8)}_{\chi_1} = 0.225 \times 10^{-3}\,\mathrm{GeV}^2$. Note that this does not contradict the result in [20], since χ_1 cannot decay into $\pi\pi$ because of parity. and the decay constant $f^{(8)}_{\chi_1}$ is therefore unconstrained in [20]. The color octet decay constant for the χ_1 being smaller than those of the $J = 0, 2$ partners is not too surprising given that the odd-spin P-wave charmonium is a somewhat different

heavy quark–antiquark system. Table 3 shows that the decay widths decrease roughly with increasing value of the baryon masses or with the reduction in the available phase space.

In Table 4, the branching ratios of the decays into $p\bar{p}$ is shown against the experimental measurements. As mentioned above, the disagreement between PDG and BES is sizable. This is true not only in the ratios of the decays into $p\bar{p}$ but also in the case of a pair of pseudoscalars in the final state. Since our results are based on a fit to the latter, until the experimental situation improves, we have to settle for our current results.

From Sect. 6 and Table 4, it is clear that only by including the color octet can the decay widths of the P-wave charmonia be brought in the range of the experimental measurements. It would be better to show this in the modified hard scattering scheme which has the advantage of the dynamical setting of renormalization scales by the process itself. But due to the complexity of the calculations, we have to revert to the standard scheme. Recall that this dynamical setting of scales is only possible if the Landau pole in α_s is suppressed by the Sudakov factor, or better yet, if it is not present at all. This suggests the use of one of the analytic models for α_s which are free from the problem of the Landau pole [31–34]. The one suggested in [33] is particularly appealing because of its relative simplicity. By combining $\alpha_s^{\text{analytic}}$ with the standard hard scattering approach, a simpler scheme than the modified one can be constructed, but which nevertheless still preserving the best features of that scheme. Under the new scheme, the amplitude would be given by

$$\mathcal{M} \sim f_{\chi_J} \phi_{\chi_J}(x) \otimes f_N \phi_N(x) \otimes f_{\bar{N}} \phi_{\bar{N}}(x)$$
$$\otimes T_{\text{H}}(x, \alpha_s^{\text{analytic}}(x)). \tag{62}$$

We have also tried to use this semi-modified scheme and again both color singlet and octet must be included. The details will be given elsewhere [35]. A somewhat similar use of this analytic α_s model in exclusive processes meant to study pion form factors can be found in [36].

Thus having satisfied ourselves with the genuine necessity and the correctness of the inclusion of the color octet state in P-wave charmonium decays, we can now generalize the arguments to even higher wave quarkonia. Remembering that the P-wave $Q\bar{Q}$ wave function has a $1/M$ suppression due to angular momentum, so one can deduce in a straightforward manner that for a D-wave, the wave function would be doubly suppressed by $1/M^2$ in relation to a S-wave. Then to calculate the exclusive decay of a D-wave quarkonium, one would need to include not only the color singlet valence state and the next higher color octet state now with the heavy fermions in a P-wave, but the next-next higher state must also be included for a consistent calculation.

Finally, as mentioned in the introduction, the nucleon wave function constructed from QCD sum rules has large disagreements with the magnetic form factor measurements below $50 \, \text{GeV}^2$. Therefore, while lacking an alternative method to derive the wave function in a fundamental way, we will have to satisfy ourselves with phenomenological constructions. We have shown together with [11] that the wave function thus constructed and its generalization to the flavor octet and decuplet baryons provide a set of reasonable model wave functions. They would no doubt provide a useful basis for the future study of other exclusive processes involving baryons at moderate Q^2.

A Basic graphs and contributions for color octet

A.1 Group 1

Basic Propagators:

$$\frac{1}{(2m_c)^2} \quad \frac{1}{x_3(1-y_1)(2m_c)^2} \quad \frac{1}{x_1 y_1 (2m_c)^2} \quad \frac{1}{(1-x_1)(1-y_1)(2m_c)^2} \quad \frac{1}{x_3 y_3 (2m_c)^2}$$

Fig. 7. Basic graph of Group 1

Table 5a. Numerators of the graphs of group 1 with helicity $(+,+,-)$

I.P.	Num. for graphs of Group 1 with $(\lambda_1, \lambda_2, \lambda_3) = (+,+,-)$	
	$J = 1$	$J = 2$
U3	$\emptyset$	$\emptyset$
L3	$\sqrt{2}(x_3 - z)(y_3 - z)(1 + y_1 - z)$	
U2	$-\frac{4\sqrt{2}}{3} x_3\{(x_2 - z)(1 + y_1 - z) - (-1)^J 2z(x_1 - y_1)\}$	
M2	$-\frac{4\sqrt{2}}{3} x_3(x_3 - z)(1 + y_1 - z)$	
L2	$\frac{\sqrt{2}}{3}(x_3 - z)(y_2 - z)(1 + y_1 - z)$	
U1	$\frac{4\sqrt{2}}{3} x_3\{(x_1 - z)(1 - y_1 - 2z) + (-1)^J z(x_1 - y_1 + 3(1 - z))\}$	
L1	$-\frac{4\sqrt{2}}{3} x_3\{(1 + y_1 - 2z)(y_1 - z) - (-1)^J z(1 - 2y_1 + z)\}$	
G3	$-\sqrt{2}(x_3 - y_3)(x_3 - z)(1 + y_1 - z)$	
G2	$\frac{4\sqrt{2}}{3} x_3\{2(1 - z^2) - y_1(3 + y_1 - 6z) + x_1(3 - y_1 - 2z)$ $-(-1)^J 2(x_1 - y_1)(1 - y_1 - 2z)\}$	
G1	$\frac{4\sqrt{2}}{3} x_3\{2(x_1 - y_1)(1 + y_1 - 2z)$ $+(-1)^J(2z(2 - z) + x_1(1 - y_1 + 2z) + y_1(3 - y_1 - 6z))\}$	
4G	$\emptyset$	$-\frac{16\sqrt{2}}{3} x_3$

Table 5b. Numerators of the graphs of group 1 with helicity $(+,-,+)$

I.P.	Num. for graphs of Group 1 with $(\lambda_1, \lambda_2, \lambda_3) = (+,-,+)$	
	$J = 1$	$J = 2$
U3	$\emptyset$	$\emptyset$
L3	$(+,+,-) + (-,+,+)$	
U2	$-\frac{4\sqrt{2}}{3} x_3(x_2 - z)(1 + y_1 - z)$	
M2	$-\frac{4\sqrt{2}}{3} x_3\{(x_3 - z)(1 + y_1 - z) + (-1)^J 2(x_1 - y_1)(1 - y_1 - z)\}$	
L2	$\frac{\sqrt{2}}{3}(x_3 - z)(y_2 - z)(1 + y_1 - z)$	
U1	$\frac{4\sqrt{2}}{3} x_3\{(x_1 - z)(1 - y_1 - 2z) + (-1)^J z(x_1 - y_1 + 3(1 - z))\}$	
L1	$-\frac{4\sqrt{2}}{3} x_3\{(1 + y_1 - 2z)(y_1 - z) - (-1)^J z(1 - 2y_1 + z)\}$	
G3	$(+,+,-) + (-,+,+)$	
G2	$\frac{4\sqrt{2}}{3} x_3\{2(1 - z^2) - y_1(3 + y_1 - 6z) + x_1(3 - y_1 - 2z)$ $-(-1)^J 2(x_1 - y_1)(1 - y_1 - 2z)\}$	
G1	$\frac{4\sqrt{2}}{3} x_3\{2(x_1 - y_1)(1 + y_1 - 2z)$ $+(-1)^J(2z(2 - z) + x_1(1 - y_1 + 2z) + y_1(3 - y_1 - 6z))\}$	
4G	$\emptyset$	$-\frac{16\sqrt{2}}{3} x_3$

Table 5c. Numerators and the additional propagators of the graphs of group 1 with helicity $(-,+,+)$

I.P.	Num. for graphs of Group 1 with $(\lambda_1, \lambda_2, \lambda_3) = (-,+,+)$		X-Prop.
	$J = 1$	$J = 2$	
U3	$\emptyset$	$\emptyset$	n.g.
L3	$-(-1)^J 2\sqrt{2} z (x_1 - y_1)(1 - y_1 - z)$		$\frac{1}{-z(y_3-z)(2m_c)^2}$
U2	$\emptyset$	$\emptyset$	$\frac{1}{-z(x_2-z)(2m_c)^2}$
M2	$\emptyset$	$\emptyset$	$\frac{1}{x_3(1-y_1)(2m_c)^2}$
L2	$(-1)^J \frac{2\sqrt{2}}{3} z (x_1 - y_1)(1 - y_1 - z)$		$\frac{1}{-z(y_2-z)(2m_c)^2}$
U1	$\emptyset$	$\emptyset$	$\frac{1}{-z(x_1-z)(2m_c)^2}$
L1	$\emptyset$	$\emptyset$	$\frac{1}{-z(y_1-z)(2m_c)^2}$
G3	$-(-1)^J \sqrt{2}(x_1 - y_1)(x_3 + z)(1 - y_1 - z)$		$\frac{1}{x_3 y_3 (2m_c)^2}$
G2	$\emptyset$	$\emptyset$	$\frac{1}{(1-x_1)(1-y_1)(2m_c)^2}$
G1	$\emptyset$	$\emptyset$	$\frac{1}{x_1 y_1 (2m_c)^2}$
4G	$\emptyset$	$\emptyset$	$\frac{1}{(2m_c)^2}$

A.2 Group 2 and group 2'

A.2.1 Group 2

Basic Propagators:

$$\frac{1}{(2m_c)^2} \quad \frac{1}{(1-y_1)(2m_c)^2} \quad \frac{1}{(1-x_1)(1-y_1)(2m_c)^2} \quad \frac{1}{x_3(1-y_1)(2m_c)^2} \quad \frac{1}{x_3 y_3 (2m_c)^2}$$
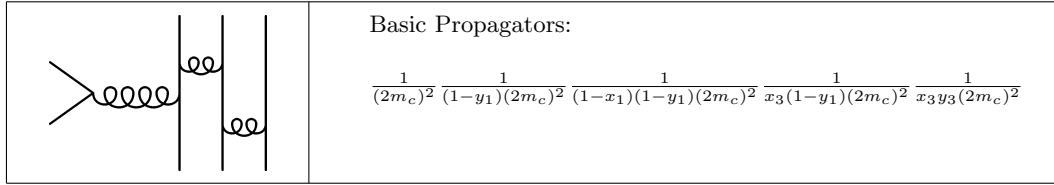
Fig. 8. Basic graph of Group 2

Table 6a. Numerators of the graphs of group 2 with helicity $(+,+,-)$ and $(+,-,+)$

I.P.	Num. for graphs of Group 2 with $(\lambda_1, \lambda_2, \lambda_3)$			
	$(+,+,-)$		$(+,-,+)$	
	$J = 1$	$J = 2$	$J = 1$	$J = 2$
U3	$\emptyset$	$\emptyset$	$\emptyset$	$\emptyset$
L3	$\emptyset$	$\emptyset$	$-(-1)^J \frac{32\sqrt{2}}{27} z (1 - y_1 - z)^2$	
U2	$(-1)^J \frac{40\sqrt{2}}{27} x_3 z (1 - y_1 - z)$		$\emptyset$	$\emptyset$
M2	$\emptyset$	$\emptyset$	$-(-1)^J \frac{32\sqrt{2}}{27} x_3 (1 - y_1 - z)^2$	
L2	$\emptyset$	$\emptyset$	$\emptyset$	$\emptyset$
U1	$(-1)^J \frac{8\sqrt{2}}{27} x_3 z (1 - y_1 - z)$			
M1	$\emptyset$	$\emptyset$	$\emptyset$	$\emptyset$
L1	$\emptyset$	$\emptyset$	$\emptyset$	$\emptyset$
G3	$\emptyset$	$\emptyset$	$\emptyset$	$\emptyset$
G2	$\frac{4\sqrt{2}}{3} x_3 \{ (1 - z)(2(1 - y_1) - z) \newline - (-1)^J (1 - y_1 - 2z)(1 - y_1 - z) \}$			

Table 6b. Numerators and the additional propagators of the graphs of group 2 with helicity $(-,+,+)$

I.P.	Num. for graphs of Group 2 with $(\lambda_1, \lambda_2, \lambda_3) = (-,+,+)$		X-Prop.
	$J = 1$	$J = 2$	
U3	$\emptyset$	$\emptyset$	n.g.
L3	$-(-1)^J \frac{32\sqrt{2}}{27} z (1 - y_1 - z)^2$		$\frac{1}{-z(y_3-z)(2m_c)^2}$
U2	$\emptyset$	$\emptyset$	$\frac{1}{-z(x_2-z)(2m_c)^2}$
M2	$\emptyset$	$\emptyset$	$\frac{1}{x_3(1-y_1)(2m_c)^2}$
L2	$(-1)^J \frac{32\sqrt{2}}{27} z (1 - y_1 - z)^2$		$\frac{1}{-z(y_2-z)(2m_c)^2}$
U1	$\emptyset$	$\emptyset$	$\frac{1}{-z(x_1-z)(2m_c)^2}$
M1	$\emptyset$	$\emptyset$	n.g.
L1	$\emptyset$	$\emptyset$	n.g.
G3	$\emptyset$	$\emptyset$	n.g.
G2	$\emptyset$	$\emptyset$	$\frac{1}{(1-x_1)(1-y_1)(2m_c)^2}$

A.2.2 Group 2'

Basic Propagators:

$$\frac{1}{(2m_c)^2} \quad \frac{1}{(1-y_1)(2m_c)^2} \quad \frac{1}{(1-x_1)(1-y_1)(2m_c)^2} \quad \frac{1}{(1-x_1)y_3(2m_c)^2} \quad \frac{1}{x_3 y_3(2m_c)^2}$$
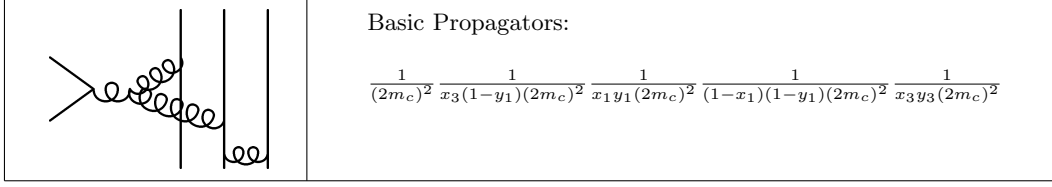
Fig. 9. Basic graph of Group 2'

Table 6a'. Numerators of the graphs of group 2' with helicity $(+,+,-)$

I.P.	Num. for graphs of Group 2' with $(\lambda_1, \lambda_2, \lambda_3) = (+,+,-)$	
	$J = 1$	$J = 2$
U3	$\frac{22\sqrt{2}}{27}(1-z)(x_3-z)(y_3-z)$	
L3	$-\frac{32\sqrt{2}}{27}(1-z)(y_3-z)^2$	
U2	$-\frac{14\sqrt{2}}{27}(1-z)(x_2-z)(y_3-z)$	
M2	$-\frac{40\sqrt{2}}{27}y_3(1-z)(y_3-z)$	
L2	$-\frac{32\sqrt{2}}{27}y_3\{(1-z)(y_2-z)+(-1)^J z(1-y_1-z)\}$	
U1	$-\frac{8\sqrt{2}}{27}y_3(1-z)(x_1-z)$	
M1	$\frac{64\sqrt{2}}{27}y_3\{(1-z)-(-1)^J(1-y_1-z)\}$	
L1	$\frac{64\sqrt{2}}{27}y_3\{y_1-z+(-1)^J z\}$	
G3	$2\sqrt{2}(1-z)(x_3-y_3)(y_3-z)$	
G2	$-\frac{4\sqrt{2}}{3}y_3\{(1-z)(x_1-y_1-3z)$ $-(-1)^J(1-x_1-2z)(1-y_1-z)\}$	

Table 6b'. Numerators of the graphs of group 2' with helicity $(+,-,+)$

I.P.	Num. for graphs of Group 2' with $(\lambda_1, \lambda_2, \lambda_3) = (+,-,+)$	
	$J = 1$	$J = 2$
U3	$(+,+,-)+(-,+,+)$	
L3	$-\frac{32\sqrt{2}}{27}(1-z)(y_3-z)^2$	
U2	$-\frac{14\sqrt{2}}{27}(1-z)(x_2-z)(y_3-z)$	
M2	$-\frac{40\sqrt{2}}{27}y_3\{(1-z)(y_3-z)$ $-(-1)^J(1-x_1-z)(1-y_1-z)\}$	
L2	$-\frac{32\sqrt{2}}{27}y_3(1-z)(y_2-z)$	
U1	$-\frac{8\sqrt{2}}{27}y_3(1-z)(x_1-z)$	
M1	$\frac{64\sqrt{2}}{27}y_3\{(1-z)-(-1)^J(1-y_1-z)\}$	
L1	$\frac{64\sqrt{2}}{27}y_3\{y_1-z+(-1)^J z\}$	
G3	$(+,+,-)+(+,-,+)$	
G2	$-\frac{4\sqrt{2}}{3}y_3\{(1-z)(x_1-y_1-3z)$ $-(-1)^J(1-x_1-2z)(1-y_1-z)\}$	

Table 6c'. Numerators and the additional propagators of the graphs of group 2' with helicity $(-,+,+)$

I.P.	Num. for graphs of Group 2' with $(\lambda_1, \lambda_2, \lambda_3) = (-,+,+)$		X-Prop.
	$J = 1$	$J = 2$	
U3	$(-1)^J \frac{22\sqrt{2}}{27}z(1-x_1-z)(1-y_1-z)$		$\frac{1}{-z(x_3-z)(2m_c)^2}$
L3	$\emptyset$	$\emptyset$	$\frac{1}{-z(y_3-z)(2m_c)^2}$
U2	$(-1)^J \frac{14\sqrt{2}}{27}z(1-x_1-z)(1-y_1-z)$		$\frac{1}{-z(x_2-z)(2m_c)^2}$
M2	$\emptyset$	$\emptyset$	$\frac{1}{(1-x_1)y_3(2m_c)^2}$
L2	$\emptyset$	$\emptyset$	$\frac{1}{-z(y_2-z)(2m_c)^2}$
U1	$\emptyset$	$\emptyset$	$\frac{1}{-z(x_1-z)(2m_c)^2}$
M1	$\emptyset$	$\emptyset$	$\frac{1}{(1-y_1)(2m_c)^2}$
L1	$\emptyset$	$\emptyset$	$\frac{1}{-z(y_1-z)(2m_c)^2}$
G3	$(-1)^J \sqrt{2}(1-x_1-z)(1-y_1-z)(y_3+z)$		$\frac{1}{x_3 y_3(2m_c)^2}$
G2	$\emptyset$	$\emptyset$	$\frac{1}{(1-x_1)(1-y_1)(2m_c)^2}$

A.3 Group 3

Basic Propagators:

$$\frac{1}{\{(z_1-x_1)(z_1-y_1)-1/4\}(2m_c)^2} \frac{1}{x_3(1-y_1)(2m_c)^2} \frac{1}{x_1y_1(2m_c)^2}$$
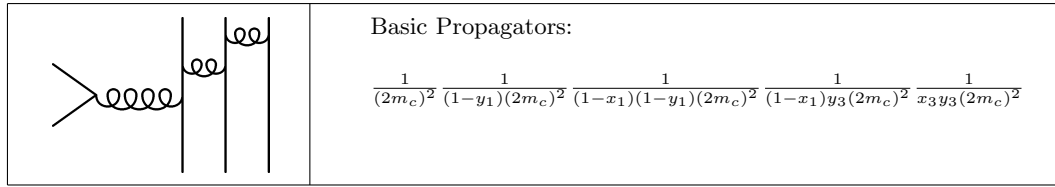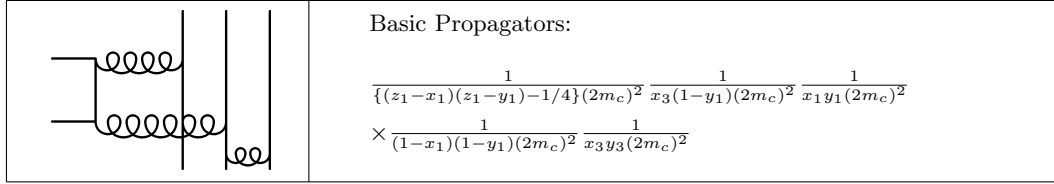$$\times \frac{1}{(1-x_1)(1-y_1)(2m_c)^2} \frac{1}{x_3y_3(2m_c)^2}$$

Fig. 10. Basic graph of Group 3

Table 7a. Numerators of the graphs of group 3 with helicity $(+,+,-)$

I.P.	Num. for graphs of Group 3 with $(\lambda_1, \lambda_2, \lambda_3) = (+,+,-)$	
	$J = 1$	$J = 2$
U3	$-\frac{10\sqrt{2}}{27}(x_3-z)^2(2y_1+z)$	
L3	$\frac{8\sqrt{2}}{27}(x_3-z)(y_3-z)(2y_1+z)$	
U2	$-\frac{4\sqrt{2}}{27}x_3\{(x_2-z)(2y_1+z)-(-1)^J 2z(x_1-y_1)\}$	
M2	$-\frac{14\sqrt{2}}{27}x_3(x_3-z)(2y_1+z)$	
L2	$-\frac{4\sqrt{2}}{27}(x_3-z)(y_2-z)(2y_1+z)$	
U1	$\frac{14\sqrt{2}}{27}x_3\{(x_1-z)(2y_1-z)+(-1)^J 2z\}$	
L1	$-\frac{4\sqrt{2}}{27}x_3\{(2y_1-z)(y_1-z)-(-1)^J 2z(1-2y_1+z)\}$	
G3	$-\frac{2\sqrt{2}}{3}(x_3-z)(x_3-y_3)(2y_1+z)$	
G2	$-\frac{\sqrt{2}}{3}x_3\{(x_1+y_1-2z)(2y_1+z)-2(2x_1+z)$ $+(-1)^J(x_1-y_1)(1-y_1-2z)\}$	
G1	$\frac{2\sqrt{2}}{3}x_3\{(x_1-y_1)(2y_1-z)$ $-(-1)^J((x_1+z)(2y_1-z)-(x_1+y_1+2z))\}$	
Q	$-\frac{\sqrt{2}}{27}x_3\{\frac{1}{2}(2y_1+z)(2y_1-z)-(x_1+y_1+z)$ $+(-1)^J\left(\frac{1}{2}(2x_1+z)(2y_1-z)-(x_1+y_1+z)\right)\}$	

Table 7b. Numerators of the graphs of group 3 with helicity $(+,-,+)$

I.P.	Num. for graphs of Group 3 with $(\lambda_1, \lambda_2, \lambda_3) = (+,-,+)$	
	$J = 1$	$J = 2$
U3	$-\frac{10\sqrt{2}}{27}(x_3-z)^2(2y_1+z)$	
L3	$\frac{8\sqrt{2}}{27}\{(x_3-z)(y_3-z)(2y_1+z)-(-1)^J 2z(x_1-y_1)(1-y_1-z)\}$	
U2	$-\frac{4\sqrt{2}}{27}x_3(x_2-z)(2y_1+z)$	
M2	$-\frac{14\sqrt{2}}{27}x_3\{(x_3-z)(2y_1+z)+(-1)^J 2(x_1-y_1)(1-y_1-z)\}$	
L2	$-\frac{4\sqrt{2}}{27}(x_3-z)(y_2-z)(2y_1+z)$	
U1	$\frac{14\sqrt{2}}{27}x_3\{(x_1-z)(2y_1-z)+(-1)^J 2z\}$	
L1	$-\frac{4\sqrt{2}}{27}x_3\{(2y_1-z)(y_1-z)-(-1)^J 2z(1-2y_1+z)\}$	
G3	$(+,+,-)+(-,+,+)$	
G2	$-\frac{\sqrt{2}}{3}x_3\{(x_1+y_1-2z)(2y_1+z)-2(2x_1+z)$ $+(-1)^J(x_1-y_1)(1-y_1-2z)\}$	
G1	$\frac{2\sqrt{2}}{3}x_3\{(x_1-y_1)(2y_1-z)$ $-(-1)^J((x_1+z)(2y_1-z)-(x_1+y_1+2z))\}$	
Q	$-\frac{\sqrt{2}}{27}x_3\{\frac{1}{2}(2y_1+z)(2y_1-z)-(x_1+y_1+z)$ $+(-1)^J\left(\frac{1}{2}(2x_1+z)(2y_1-z)-(x_1+y_1+z)\right)\}$	

Table 7c. Numerators and the additional propagators of the graphs of group 3 with helicity $(-,+,+)$

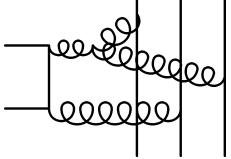| I.P.	Num. for graphs of Group 3 with $(\lambda_1, \lambda_2, \lambda_3) = (-,+,+)$		X-Prop.
	$J = 1$	$J = 2$	
U3	$\emptyset$	$\emptyset$	$\frac{1}{-z(x_3-z)(2m_c)^2}$
L3	$-(-1)^J \frac{16\sqrt{2}}{27} z(x_1 - y_1)(1 - y_1 - z)$		$\frac{1}{-z(y_3-z)(2m_c)^2}$
U2	$\emptyset$	$\emptyset$	$\frac{1}{-z(x_2-z)(2m_c)^2}$
M2	$\emptyset$	$\emptyset$	$\frac{1}{x_3(1-y_1)(2m_c)^2}$
L2	$-(-1)^J \frac{8\sqrt{2}}{27} z(x_1 - y_1)(1 - y_1 - z)$		$\frac{1}{-z(y_2-z)(2m_c)^2}$
U1	$\emptyset$	$\emptyset$	$\frac{1}{-z(x_1-z)(2m_c)^2}$
L1	$\emptyset$	$\emptyset$	$\frac{1}{-z(y_1-z)(2m_c)^2}$
G3	$-(-1)^J \frac{2\sqrt{2}}{3}(x_3 + z)(x_1 - y_1)(1 - y_1 - z)$		$\frac{1}{x_3 y_3 (2m_c)^2}$
G2	$\emptyset$	$\emptyset$	$\frac{1}{(1-x_1)(1-y_1)(2m_c)^2}$
G1	$\emptyset$	$\emptyset$	$\frac{1}{x_1 y_1 (2m_c)^2}$
Q	$\emptyset$	$\emptyset$	$\frac{1}{[(x_1-z_1)(y_1-z_1)-1/4](2m_c)^2}$

A.4 Group 4

Basic Propagators:

$$\frac{1}{\{(z_2-x_2)(z_2-y_2)-1/4\}(2m_c)^2} \frac{1}{(1-x_2)(1-y_2)(2m_c)^2+\rho^2} \frac{1}{x_1 y_1 (2m_c)^2}$$

$$\times \frac{1}{x_2 y_2 (2m_c)^2} \frac{1}{x_3 y_3 (2m_c)^2}$$

Fig. 11. Basic graph of Group 4

Table 8a. Numerators of the graphs of group 4 with helicity $(+,+,-)$ and $(+,-,+)$

I.P.	Num. for graphs of Group 4 with$(\lambda_1, \lambda_2, \lambda_3)$			
	$(+,+,-)$		$(+,-,+)$	
	$J=1$	$J=2$	$J=1$	$J=2$
U3	$-\frac{\sqrt{2}}{3}(x_3-z)\{(x_1-x_3+z)+(y_1-y_3+z)$ $-2(x_1-x_3+z)(z_2-y_2)$ $-2(y_1-y_3+z)(z_2-x_2)\}$		$(-1)^J\frac{2\sqrt{2}}{3}z(x_2-y_2)(2x_1+x_3-z)$	
L3	$\frac{\sqrt{2}}{12}(y_3-z)\{(x_1-x_3+z)+(y_1-y_3+z)$ $-2(x_1-x_3+z)(z_2-y_2)$ $-2(y_1-y_3+z)(z_2-x_2)\}$		$(-1)^J\frac{\sqrt{2}}{6}z(x_2-y_2)(2y_1+y_3-z)$	
U2	$\emptyset$	$\emptyset$	$\emptyset$	$\emptyset$
L2	$\emptyset$	$\emptyset$	$\emptyset$	$\emptyset$
U1	$(+,-,+)+(-,+,+)$		$(-1)^J\frac{2\sqrt{2}}{3}z(x_2-y_2)(x_1+2x_3-z)$	
L1	$(+,-,+)+(-,+,+)$		$(-1)^J\frac{\sqrt{2}}{6}z(x_2-y_2)(y_1+2y_3-z)$	
G3	$-\frac{5\sqrt{2}}{12}(x_3-y_3)\{(x_1-x_3+z)+(y_1-y_3+z)$ $-2(x_1-x_3+z)(z_2-y_2)$ $-2(y_1-y_3+z)(z_2-x_2)\}$		$(-1)^J\frac{5\sqrt{2}}{12}(x_2-y_2)$ $\times\ \{(2x_1+x_3-z)(y_3+z)$ $(2y_1+y_3-z)(x_3+z)\}$	
G2	$\emptyset$	$\emptyset$	$\emptyset$	$\emptyset$
G1	$(+,-,+)+(-,+,+)$		$(-1)^J\frac{5\sqrt{2}}{12}(x_2-y_2)$ $\times\ \{(2x_3+x_1-z)(y_1+z)$ $(2y_3+y_1-z)(x_1+z)\}$	
GR	$\emptyset$	$\emptyset$	$\emptyset$	$\emptyset$
4G	$-\frac{5}{\sqrt{2}}(x_2-y_2)$	$-\frac{5}{3\sqrt{2}}(x_2-y_2)$	$-(-1)^J\frac{5\sqrt{2}}{3}(x_2-y_2)$	
Q	$\emptyset$	$\emptyset$	$\emptyset$	$\emptyset$

Table 8b. Numerators and the additional propagators of the graphs of group 4 with helicity $(-,+,+)$

I.P.	Num. for graphs of Group 4 with $(\lambda_1, \lambda_2, \lambda_3) = (-,+,+)$		X-Prop.
	$J=1$	$J=2$	
U3	$(+,+,-)+(+,-,+)$		$\frac{1}{-z(x_3-z)(2m_c)^2}$
L3	$(+,+,-)+(+,-,+)$		$\frac{1}{-z(y_3-z)(2m_c)^2}$
U2	$\emptyset$	$\emptyset$	n.g.
L2	$\emptyset$	$\emptyset$	n.g.
U1	$-\frac{\sqrt{2}}{3}(x_1-z)\{(x_3-x_1+z)+(y_3-y_1+z)$ $-2(x_3-x_1+z)(z_2-y_2)$ $-2(y_3-y_1+z)(z_2-x_2)\}$		$\frac{1}{-z(x_1-z)(2m_c)^2}$
L1	$\frac{\sqrt{2}}{12}(y_1-z)\{(x_3-x_1+z)+(y_3-y_1+z)$ $-2(x_3-x_1+z)(z_2-y_2)$ $-2(y_3-y_1+z)(z_2-x_2)\}$		$\frac{1}{-z(y_1-z)(2m_c)^2}$
G3	$(+,+,-)+(+,-,+)$		$\frac{1}{x_3y_3(2m_c)^2}$
G2	$\emptyset$	$\emptyset$	n.g.
G1	$-\frac{5\sqrt{2}}{12}(x_1-y_1)\{(x_3-x_1+z)+(y_3-y_1+z)$ $-2(x_3-x_1+z)(z_2-y_2)$ $-2(y_3-y_1+z)(z_2-x_2)\}$		$\frac{1}{x_1y_1(2m_c)^2}$
GR	$\emptyset$	$\emptyset$	n.g.
4G	$-\frac{5}{\sqrt{2}}(x_2-y_2)$	$-\frac{5}{3\sqrt{2}}(x_2-y_2)$	$\frac{1}{(2m_c)^2}$
Q	$\emptyset$	$\emptyset$	n.g.

A.5 Group 5

Basic Propagators:

$$\frac{1}{\{(z_1-x_1)(z_1-y_1)-1/4\}(2m_c)^2} \frac{1}{\{(z_2-x_3)(z_2-y_3)-1/4\}(2m_c)^2} \frac{1}{x_1 y_1 (2m_c)^2}$$

$$\times \frac{1}{x_2 y_2 (2m_c)^2} \frac{1}{x_3 y_3 (2m_c)^2}$$
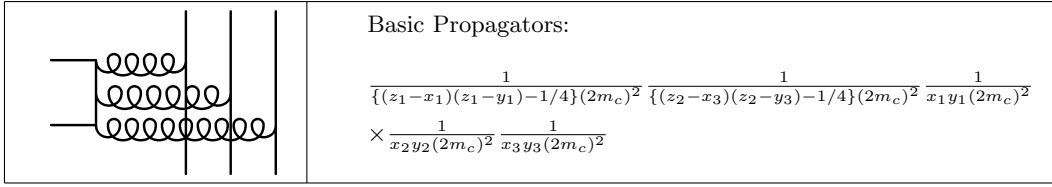
Fig. 12. Basic graph of Group 5

Table 9a. Numerators of the graphs of group 5 with helicity $(+,+,-)$

I.P.	Num. for graphs of Group 5 with $(\lambda_1,\lambda_2,\lambda_3)=(+,+,-)$	
	$J=1$	$J=2$
U3	$\emptyset$	$\emptyset$
L3	$\emptyset$	$\emptyset$
U2	$-(-1)^J \frac{\sqrt{2}}{12} z (2x_1+z)(2x_3+z)$	
L2	$-(-1)^J \frac{\sqrt{2}}{12} z (2y_1+z)(2y_3+z)$	
U1	$(-1)^J \frac{\sqrt{2}}{4} z \{1 - 2x_2 - 4(x_2+x_3-z_1)(y_3-z_1)\}$	
L1	$-(-1)^J \frac{\sqrt{2}}{6} z \{1 - 2y_2 - 4(y_2+y_3-z_1)(x_3-z_1)\}$	
G3	$\emptyset$	$\emptyset$
G2	$\emptyset$	$\emptyset$
G1	$-(-1)^J \frac{5}{12\sqrt{2}} \{(x_1-y_1)(1-4(x_3-z_1)(y_3-z_1)) \\ +2x_2(2y_3+z)(y_1+z) \\ -2y_2(2x_3+z)(x_1+z)\}$	
UQ	$-(-1)^J \frac{5\sqrt{2}}{108} \{(x_3-y_3) - 2z(x_2-y_2) + 4(x_1-y_1)(1-z_1)^2 \\ -4(x_1(1-x_3)-x_2 z_1)(1-y_1-z_1) \\ +4(y_1(1-y_3)-y_2 z_1)(1-x_1-z_1)\}$	
LQ	$\emptyset$	$\emptyset$

Table 9b. Numerators of the graphs of group 5 with helicity $(+,-,+)$

I.P.	Num. for graphs of Group 5 with $(\lambda_1, \lambda_2, \lambda_3) = (+,-,+)$	
	$J = 1$	$J = 2$
U3	$-\frac{\sqrt{2}}{6}\{2(x_3 - z)[1 - x_2 - y_2 - 2(1 - x_3 - z_1)(y_1 - z_1)$ $- 2(1 - y_3 - z_1)(x_1 - z_1)]$ $+(-1)^J z[1 - 2x_2 - 4(1 - x_3 - z_1)(y_1 - z_1)]\}$	
L3	$\frac{\sqrt{2}}{4}\{2(y_3 - z)[1 - x_2 - y_2 - 2(1 - x_3 - z_1)(y_1 - z_1)$ $- 2(1 - y_3 - z_1)(x_1 - z_1)]$ $+(-1)^J z[1 - 2y_2 - 4(1 - y_3 - z_1)(x_1 - z_1)]\}$	
U2	$-\frac{\sqrt{2}}{6}(x_2 - z)\{1- (x_2 + y_2 - 2z)$ $+2(x_3 - z_1)(y_1 - z_1)+2(y_3 - z_1)(x_1 - z_1)\}$	
L2	$-\frac{\sqrt{2}}{6}(y_2 - z)\{1- (x_2 + y_2 - 2z)$ $+2(x_3 - z_1)(y_1 - z_1)+2(y_3 - z_1)(x_1 - z_1)\}$	
U1	$\frac{\sqrt{2}}{4}\{2(x_1 - z)[1 - x_2 - y_2 - 2(1 - x_1 - z_1)(y_3 - z_1)$ $- 2(1 - y_1 - z_1)(x_3 - z_1)]$ $+(-1)^J z[1 - 2x_2 - 4(1 - x_1 - z_1)(y_3 - z_1)]\}$	
L1	$-\frac{\sqrt{2}}{6}\{2(y_1 - z)[1 - x_2 - y_2 - 2(1 - x_1 - z_1)(y_3 - z_1)$ $- 2(1 - y_1 - z_1)(x_3 - z_1)]$ $+(-1)^J z[1 - 2y_2 - 4(1 - y_1 - z_1)(x_3 - z_1)]\}$	
G3	$-\frac{5}{12\sqrt{2}}\{4(x_3 - y_3)[1 - y_2 - x_2(2y_1 + z) - 2(x_1 - z_1)(y_1 - y_3 + z)]$ $-(-1)^J[2z(x_2(2y_1 + z) - y_2(2x_1 + z))$ $+x_3(1 - 2y_2 - 4(x_1 - z_1)(1 - y_3 - z_1))$ $-y_3(1 - 2x_2 - 4(y_1 - z_1)(1 - x_3 - z_1))]\}$	
G2	$\emptyset$	$\emptyset$
G1	$\frac{5}{12\sqrt{2}}\{4(x_1 - y_1)[1 - y_2 - x_2(2y_3 + z) + 2(x_3 - z_1)(y_1 - y_3 - z)]$ $-(-1)^J[2z(x_2(2y_3 + z) - y_2(2x_3 + z))$ $+x_1(1 - 2y_2 - 4(x_3 - z_1)(1 - y_1 - z_1))$ $-y_1(1 - 2x_2 - 4(y_3 - z_1)(1 - x_1 - z_1))]\}$	
UQ	$-\frac{5\sqrt{2}}{108}\{z(2 + z)(x_1 - y_1) + (z(2 - z) + 2(x_1 + y_1))(x_2 - y_2)$ $+4(z_1 - y_3)x_1^2 - 4(z_1 - x_3)y_1^2\}$	
LQ	$\frac{5\sqrt{2}}{108}\{z(2 + z)(x_3 - y_3) + (z(2 - z) + 2(x_3 + y_3))(x_2 - y_2)$ $+4(z_1 - y_1)x_3^2 - 4(z_1 - x_1)y_3^2\}$	

Table 9c. Numerators and the additional propagators of the graphs of group 5 with helicity $(-,+,+)$

I.P.	Num. for graphs of Group 5 with $(\lambda_1,\lambda_2,\lambda_3)=(-,+,+)$		X-Prop.
	$J=1$	$J=2$	
U3	$-(-1)^J\frac{\sqrt2}{6}z\{1-2x_2-4(x_1+x_2-z_1)(y_1-z_1)\}$		$\frac{1}{-z(x_3-z)(2m_c)^2}$
L3	$(-1)^J\frac{\sqrt2}{4}z\{1-2y_2-4(y_1+y_2-z_1)(x_1-z_1)\}$		$\frac{1}{-z(y_3-z)(2m_c)^2}$
U2	$-(-1)^J\frac{\sqrt2}{12}z(2x_1+z)(2x_3+z)$		$\frac{1}{-z(x_2-z)(2m_c)^2}$
L2	$-(-1)^J\frac{\sqrt2}{12}z(2y_1+z)(2y_3+z)$		$\frac{1}{-z(y_2-z)(2m_c)^2}$
U1	$\emptyset$	$\emptyset$	$\frac{1}{-z(x_1-z)(2m_c)^2}$
L1	$\emptyset$	$\emptyset$	$\frac{1}{-z(y_1-z)(2m_c)^2}$
G3	$(-1)^J\frac{5}{12\sqrt2}\{(x_3-y_3)(1-4(x_1-z_1)(y_1-z_1))$ $+2x_2(2y_1+z)(y_3+z)$ $-2y_2(2x_1+z)(x_3+z)\}$		$\frac{1}{x_3y_3(2m_c)^2}$
G2	$\emptyset$	$\emptyset$	n.g.
G1	$\emptyset$	$\emptyset$	$\frac{1}{x_1y_1(2m_c)^2}$
UQ	$\emptyset$	$\emptyset$	$\frac{1}{[(x_1-z_1)(y_1-z_1)-1/4](2m_c)^2}$
LQ	$(-1)^J\frac{5\sqrt2}{108}\{(x_1-y_1)-2z(x_2-y_2)+4(x_3-y_3)(1-z_1)^2$ $-4(x_3(1-x_1)-x_2z_1)(1-y_3-z_1)$ $+4(y_3(1-y_1)-y_2z_1)(1-x_3-z_1)\}$		$\frac{1}{[(x_3-z_1)(y_3-z_1)-1/4](2m_c)^2}$

A.6 Group 6

Basic Propagators:

$$\frac{1}{(2m_c)^4}\ \frac{1}{x_1y_1(2m_c)^2}\ \frac{1}{x_2y_2(2m_c)^2}\ \frac{1}{x_3y_3(2m_c)^2}$$

Fig. 13. Basic graph of Group 6

Table 10a. Numerators of the graphs of group 6 with helicity $(+,+,-)$ and $(+,-,+)$

I.P.	Num. for graphs of Group 6 with $(\lambda_1,\lambda_2,\lambda_3)$			
	$(+,+,-)$		$(+,-,+)$	
	$J=1$	$J=2$	$J=1$	$J=2$
U3	$2\sqrt2(x_3-z)$		$-\sqrt2\{x_3-z+(-1)^J2z\}$	
L3	$2\sqrt2(y_3-z)$		$-\sqrt2\{y_3-z+(-1)^J2z\}$	
U2	$-\sqrt2\{x_2-z+(-1)^J2z\}$		$2\sqrt2(x_2-z)$	
L2	$-\sqrt2\{y_2-z+(-1)^J2z\}$		$2\sqrt2(y_2-z)$	
U1	$-\sqrt2\{x_1-z+(-1)^J2z\}$			
L1	$-\sqrt2\{y_1-z+(-1)^J2z\}$			
G3	$\emptyset$	$\emptyset$	$\emptyset$	$\emptyset$
G2	$\emptyset$	$\emptyset$	$\emptyset$	$\emptyset$
G1	$\emptyset$	$\emptyset$	$\emptyset$	$\emptyset$

Table 10b. Numerators and the additional propagators of the graphs of group 6 with helicity $(-,+,+)$

I.P.	Num. for graphs of Group 6 with $(\lambda_1,\lambda_2,\lambda_3)=(-,+,+)$		X-Prop.
	$J=1$	$J=2$	
U3	$-\sqrt2\{x_3-z+(-1)^J2z\}$		$\frac{1}{-z(x_3-z)(2m_c)^2}$
L3	$-\sqrt2\{y_3-z+(-1)^J2z\}$		$\frac{1}{-z(y_3-z)(2m_c)^2}$
U2	$-\sqrt2\{x_2-z+(-1)^J2z\}$		$\frac{1}{-z(x_2-z)(2m_c)^2}$
L2	$-\sqrt2\{y_2-z+(-1)^J2z\}$		$\frac{1}{-z(y_2-z)(2m_c)^2}$
U1	$2\sqrt2(x_1-z)$		$\frac{1}{-z(x_1-z)(2m_c)^2}$
L1	$2\sqrt2(y_1-z)$		$\frac{1}{-z(y_1-z)(2m_c)^2}$
G3	$\emptyset$	$\emptyset$	n.g.
G2	$\emptyset$	$\emptyset$	n.g.
G1	$\emptyset$	$\emptyset$	n.g.

A.7 Group 7

Basic Propagators:

$$\frac{1}{(2m_c)^2} \ \frac{1}{(1-y_1)(2m_c)^2} \ \frac{1}{(1-x_2)y_3(2m_c)^2} \ \frac{1}{x_2y_2(2m_c)^2} \ \frac{1}{x_3y_3(2m_c)^2}$$
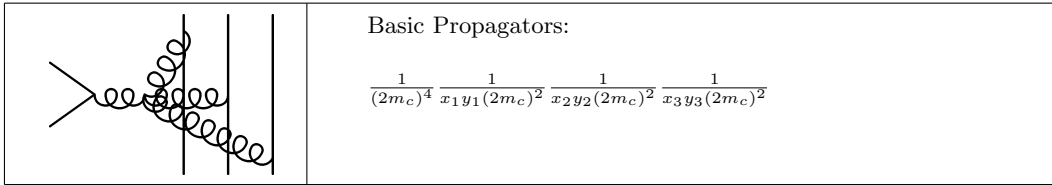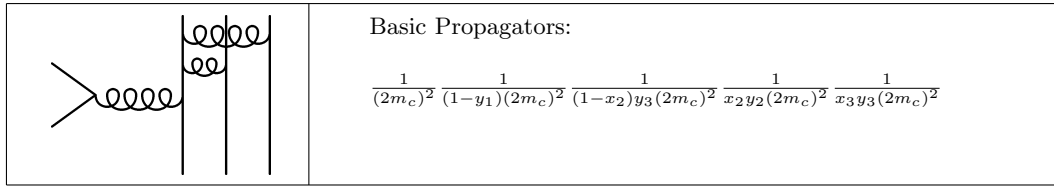
Fig. 14. Basic graph of Group 7

Table 11a. Numerators of the graphs of group 7 with helicity $(+,+,-)$ and $(+,-,+)$

I.P.	Num. for graphs of Group 7 with$(\lambda_1, \lambda_2, \lambda_3)$			
	$(+,+,-)$		$(+,-,+)$	
	$J=1$	$J=2$	$J=1$	$J=2$
U3	$\frac{14\sqrt{2}}{27}(1-z)(x_3-z)(y_3-z)$		$-(-1)^J \frac{14\sqrt{2}}{27}z(1-x_2-z)$ $\times(1-y_1-z)$	
L3	$\frac{32\sqrt{2}}{27}(1-z)(y_3-z)^2$		$\emptyset$	$\emptyset$
U2	$-\frac{40\sqrt{2}}{27}(1-z)(x_2-z)y_3$		$\emptyset$	$\emptyset$
L2	$\frac{32\sqrt{2}}{27}y_3\{(1-z)(y_2-z)$ $+(-1)^J z(1-y_1-z)\}$		$\emptyset$	$\emptyset$
U1	$\frac{26\sqrt{2}}{27}(1-z)(x_1-z)(y_3-z)$		$(-1)^J \frac{26\sqrt{2}}{27}z(1-x_2-z)$ $\times(1-y_1-z)$	
UM1	$-\frac{8\sqrt{2}}{27}y_3(1-z)(y_3-z)$		$\emptyset$	$\emptyset$
LM1	$-\frac{64\sqrt{2}}{27}y_3\{(1-z)-(-1)^J(1-y_1-z)\}$		$\emptyset$	$\emptyset$
L1	$-\frac{64\sqrt{2}}{27}y_3\{(y_1-z)+(-1)^J z\}$		$\emptyset$	$\emptyset$
G3	$-\frac{2\sqrt{2}}{3}(1-z)(x_3-y_3)(y_3-z)$		$(-1)^J \frac{\sqrt{2}}{3}(1-x_2-z)$ $\times(1-y_1-z)$ $\times(y_3+z)$	
G2	$-\frac{4\sqrt{2}}{3}y_3\{2(1-z)(x_2-y_2)$ $-(-1)^J(x_2+z)(1-y_1-z)\}$		$\emptyset$	$\emptyset$

Table 11b. Numerators and the additional propagators of the graphs of group 7 with helicity $(-,+,+)$

I.P.	Num. for graphs of Group 7 with $(\lambda_1, \lambda_2, \lambda_3)=(-,+,+)$		X-Prop.
	$J=1$	$J=2$	
U3	$-(-1)^J \frac{14\sqrt{2}}{27}z(1-x_2-z)(1-y_1-z)$		$\frac{1}{-z(x_3-z)(2m_c)^2}$
L3	$\emptyset$	$\emptyset$	$\frac{1}{-z(y_3-z)(2m_c)^2}$
U2	$\emptyset$	$\emptyset$	$\frac{1}{-z(x_2-z)(2m_c)^2}$
L2	$(-1)^J \frac{32\sqrt{2}}{27}zy_3(1-y_1-z)$		$\frac{1}{-z(y_2-z)(2m_c)^2}$
U1	$\emptyset$	$\emptyset$	$\frac{1}{-z(x_1-z)(2m_c)^2}$
UM1	$-(-1)^J \frac{8\sqrt{2}}{27}y_3(1-x_2-z)(1-y_1-z)$		$\frac{1}{(1-x_2)y_3(2m_c)^2}$
LM1	$\emptyset$	$\emptyset$	$\frac{1}{(1-y_1)(2m_c)^2}$
L1	$\emptyset$	$\emptyset$	$\frac{1}{-z(y_1-z)(2m_c)^2}$
G3	$(-1)^J \frac{\sqrt{2}}{3}(1-x_2-z)(1-y_1-z)(y_3+z)$		$\frac{1}{x_3y_3(2m_c)^2}$
G2	$(-1)^J \frac{4\sqrt{2}}{3}y_3(1-y_1-z)(x_2+z)$		$\frac{1}{x_2y_2(2m_c)^2}$

A.8 Group 8

Basic Propagators:

$$\frac{1}{(2m_c)^2} \quad \frac{1}{x_2(1-y_3)(2m_c)^2} \quad \frac{1}{(1-x_2)y_3(2m_c)^2} \quad \frac{1}{x_2y_2(2m_c)^2} \quad \frac{1}{x_3y_3(2m_c)^2}$$
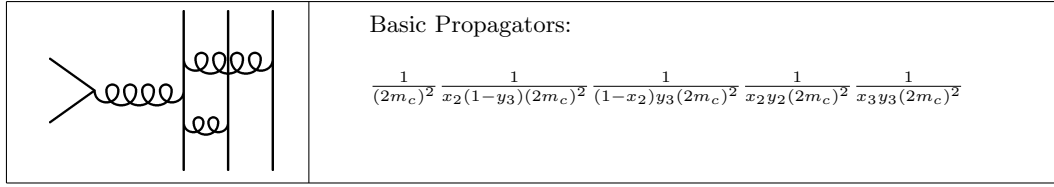
Fig. 15. Basic graph of Group 8

Table 12a. Numerators of the graphs of group 8 with helicity $(+,+,-)$ and $(+,-,+)$

I.P.	Num. for graphs of Group 8 with $(\lambda_1, \lambda_2, \lambda_3)$			
	$(+,+,-)$		$(+,-,+)$	
	$J=1$	$J=2$	$J=1$	$J=2$
U3	$\emptyset$	$\emptyset$	$(-1)^J \frac{40\sqrt{2}}{27} x_2 z(1-x_2-z)$	
L3	$\emptyset$	$\emptyset$	$\emptyset$	$\emptyset$
U2	$\emptyset$	$\emptyset$	$\emptyset$	$\emptyset$
L2	$(-1)^J \frac{40\sqrt{2}}{27} y_3 z(1-y_3-z)$		$\emptyset$	$\emptyset$
U1	$\emptyset$	$\emptyset$	$(-1)^J \frac{8\sqrt{2}}{27} x_2 z(1-x_2-z)$	
UM1	$\emptyset$	$\emptyset$	$\emptyset$	$\emptyset$
LM1	$\emptyset$	$\emptyset$	$\emptyset$	$\emptyset$
L1	$(-1)^J \frac{8\sqrt{2}}{27} y_3 z(1-y_3-z)$		$\emptyset$	$\emptyset$
G3	$\emptyset$	$\emptyset$	$(-1)^J \frac{4\sqrt{2}}{3} x_2(1-x_2-z)(y_3+z)$	
G2	$(-1)^J \frac{4\sqrt{2}}{3} y_3(1-y_3-z)(x_2+z)$		$\emptyset$	$\emptyset$

Table 12b. Numerators and the additional propagators of the graphs of group 8 with helicity $(-,+,+)$

I.P.	Num. for graphs of Group 8 with $(\lambda_1, \lambda_2, \lambda_3) = (-,+,+)$		X-Prop.
	$J=1$	$J=2$	
U3	$\frac{40\sqrt{2}}{27} x_2\{(x_3-z)(y_3-z)+(-1)^J z(1-x_2-z)\}$		$\frac{1}{-z(x_3-z)(2m_c)^2}$
L3	$-\frac{32\sqrt{2}}{27} x_2(y_3-z)^2$		$\frac{1}{-z(y_3-z)(2m_c)^2}$
U2	$-\frac{32\sqrt{2}}{27} y_3(x_2-z)^2$		$\frac{1}{-z(x_2-z)(2m_c)^2}$
L2	$\frac{40\sqrt{2}}{27} y_3\{(x_2-z)(y_2-z)+(-1)^J z(1-y_3-z)\}$		$\frac{1}{-z(y_2-z)(2m_c)^2}$
U1	$-\frac{8\sqrt{2}}{27} x_2(x_1-z)(y_3-z)$		$\frac{1}{-z(x_1-z)(2m_c)^2}$
UM1	$-\frac{64\sqrt{2}}{27} x_2 y_3\{(y_3-z)-(-1)^J(1-x_2-z)\}$		$\frac{1}{(1-x_2)y_3(2m_c)^2}$
LM1	$-\frac{64\sqrt{2}}{27} x_2 y_3\{(x_2-z)-(-1)^J(1-y_3-z)\}$		$\frac{1}{x_2(1-y_3)(2m_c)^2}$
L1	$-\frac{8\sqrt{2}}{27} y_3(x_2-z)(y_1-z)$		$\frac{1}{-z(y_1-z)(2m_c)^2}$
G3	$\frac{4\sqrt{2}}{3} x_2\{2(x_3-y_3)(y_3-z)$ $+(-1)^J(1-x_2-z)(y_3+z)\}$		$\frac{1}{x_3 y_3(2m_c)^2}$
G2	$-\frac{4\sqrt{2}}{3} y_3\{2(x_2-y_2)(x_2-z)$ $-(-1)^J(1-y_3-z)(x_2+z)\}$		$\frac{1}{x_2 y_2(2m_c)^2}$

A.9 Group 9

Basic Propagators:

$$\frac{1}{(2m_c)^2} \frac{1}{(1-x_2)(1-y_2)(2m_c)^2+\rho^2} \frac{1}{x_1y_1(2m_c)^2} \frac{1}{x_2y_2(2m_c)^2}$$

$$\times \frac{1}{x_3y_3(2m_c)^2}$$
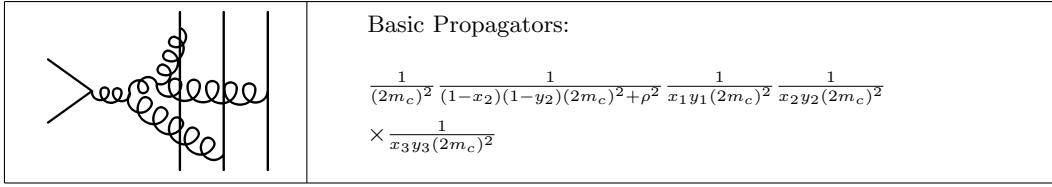
Fig. 16. Basic graph of Group 9

Table 13a. Numerators of the graphs of group 9 with helicity $(+,+,-)$ and $(+,-,+)$

I.P.	Num. for graphs of Group 9 with$(\lambda_1, \lambda_2, \lambda_3)$			
	$(+,+,-)$		$(+,-,+)$	
	$J = 1$	$J = 2$	$J = 1$	$J = 2$
U3	$-\frac{1}{\sqrt{2}}(x_3 - z)\{(1 + x_2 - z)(y_1 - y_3 + z)$ $+(1 + y_2 - z)(x_1 - x_3 + z)\}$		$(-1)^J \sqrt{2}z(x_2 - y_2)(2x_1 + x_3 - z)$	
L3	$-\frac{1}{\sqrt{2}}(y_3 - z)\{(1 + x_2 - z)(y_1 - y_3 + z)$ $+(1 + y_2 - z)(x_1 - x_3 + z)\}$		$(-1)^J \sqrt{2}z(y_2 - x_2)(2y_1 + y_3 - z)$	
U2	$\emptyset$	$\emptyset$	$\emptyset$	$\emptyset$
L2	$\emptyset$	$\emptyset$	$\emptyset$	$\emptyset$
U1	$-\sqrt{2}\{\frac{1}{2}(x_1 - z)[(1 + x_2 - z)(y_3 - y_1 + z)$ $+(1 + y_2 - z)(x_3 - x_1 + z)]$ $-(-1)^J z(x_2 - y_2)(2x_3 + x_1 - z)\}$		$(-1)^J \sqrt{2}z(x_2 - y_2)(2x_3 + x_1 - z)$	
L1	$-\sqrt{2}\{\frac{1}{2}(y_1 - z)[(1 + x_2 - z)(y_3 - y_1 + z)$ $+(1 + y_2 - z)(x_3 - x_1 + z)]$ $-(-1)^J z(y_2 - x_2)(2y_3 + y_1 - z)\}$		$(-1)^J \sqrt{2}z(y_2 - x_2)(2y_3 + y_1 - z)$	
G3	$\emptyset$	$\emptyset$	$\emptyset$	$\emptyset$
G2	$\emptyset$	$\emptyset$	$\emptyset$	$\emptyset$
G1	$\emptyset$	$\emptyset$	$\emptyset$	$\emptyset$
GR	$\emptyset$	$\emptyset$	$\emptyset$	$\emptyset$
4G1	$\emptyset$	$\emptyset$	$\emptyset$	$\emptyset$
4G2	$\emptyset$	$\emptyset$	$\emptyset$	$\emptyset$

Table 13b. Numerators and the additional propagators of the graphs of group 9 with helicity $(-, +, +)$

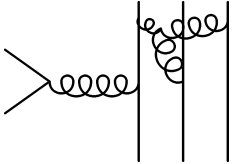| I.P.	Num. for graphs of Group 9 with $(\lambda_1, \lambda_2, \lambda_3) = (-, +, +)$		X-Prop.
	$J = 1$	$J = 2$	
U3	$-\sqrt{2}\left\{\frac{1}{2}(x_3 - z)[(1 + x_2 - z)(y_1 - y_3 + z)\right.$ $+(1 + y_2 - z)(x_1 - x_3 + z)]$ $\left.-(-1)^J z(x_2 - y_2)(2x_1 + x_3 - z)\right\}$		$\frac{1}{-z(x_3-z)(2m_c)^2}$
L3	$-\sqrt{2}\left\{\frac{1}{2}(y_3 - z)[(1 + x_2 - z)(y_1 - y_3 + z)\right.$ $+(1 + y_2 - z)(x_1 - x_3 + z)]$ $\left.-(-1)^J z(y_2 - x_2)(2y_1 + y_3 - z)\right\}$		$\frac{1}{-z(y_3-z)(2m_c)^2}$
U2	$\emptyset$	$\emptyset$	n.g.
L2	$\emptyset$	$\emptyset$	n.g.
U1	$-\frac{1}{\sqrt{2}}(x_1 - z)\{(1 + x_2 - z)(y_3 - y_1 + z)$ $+(1 + y_2 - z)(x_3 - x_1 + z)\}$		$\frac{1}{-z(x_1-z)(2m_c)^2}$
L1	$-\frac{1}{\sqrt{2}}(y_1 - z)\{(1 + x_2 - z)(y_3 - y_1 + z)$ $+(1 + y_2 - z)(x_3 - x_1 + z)\}$		$\frac{1}{-z(y_1-z)(2m_c)^2}$
G3	$\emptyset$	$\emptyset$	n.g.
G2	$\emptyset$	$\emptyset$	n.g.
G1	$\emptyset$	$\emptyset$	n.g.
GR	$\emptyset$	$\emptyset$	n.g.
4G1	$\emptyset$	$\emptyset$	none
4G2	$\emptyset$	$\emptyset$	none

A.10 Group 10

Basic Propagators:

$$\frac{1}{(2m_c)^2} \frac{1}{(1-y_1)(2m_c)^2} \frac{1}{(1-x_1)(1-y_1)(2m_c)^2+\rho^2} \frac{1}{x_2 y_2 (2m_c)^2}$$

$$\times \frac{1}{x_3 y_3 (2m_c)^2}$$

Fig. 17. Basic graph of Group 10

Table 14a. Numerators of the graphs of group 10 with helicity $(+,+,-)$ and $(+,-,+)$

I.P.	Num. for graphs of Group 10 with $(\lambda_1, \lambda_2, \lambda_3)$			
	$(+,+,-)$		$(+,-,+)$	
	$J = 1$	$J = 2$	$J = 1$	$J = 2$
U3	$\sqrt{2}(1-z)(x_3-z)(y_3-y_2-z)$		$\sqrt{2}\{(1-z)(x_3-z)(y_3-y_2-z)$ $+(-1)^J z(y_2+y_3-z)(2x_2+x_3-z)\}$	
L3	$\emptyset$	$\emptyset$	$\emptyset$	$\emptyset$
U2	$\sqrt{2}\{(1-z)(x_2-z)(y_2-y_3-z)$ $+(-1)^J z(y_2+y_3-z)(2x_3+x_2-z)\}$		$\sqrt{2}(1-z)(x_2-z)(y_2-y_3-z)$	
L2	$\emptyset$	$\emptyset$	$\emptyset$	$\emptyset$
U1	$\emptyset$	$\emptyset$	$\emptyset$	$\emptyset$
M1	$\emptyset$	$\emptyset$	$\emptyset$	$\emptyset$
L1	$\emptyset$	$\emptyset$	$\emptyset$	$\emptyset$
G3	$\sqrt{2}(1-z)(x_3-y_3)(y_3-y_2-z)$		$\sqrt{2}\{(1-z)(x_3-y_3)(y_3-y_2-z)$ $+(-1)^J(y_2+y_3-z)$ $\times(x_3y_2+x_2y_3+x_3y_3$ $+z(x_2+y_2-z))\}$	
G2	$\sqrt{2}\{(1-z)(x_2-y_2)(y_2-y_3-z)$ $+(-1)^J(y_2+y_3-z)$ $\times(x_3y_2+x_2y_3+x_2y_2$ $+z(x_3+y_3-z))\}$		$\sqrt{2}(1-z)(x_2-y_2)(y_2-y_3-z)$	
GR	$\emptyset$	$\emptyset$	$\emptyset$	$\emptyset$
4G	$\sqrt{2}\{2(1-z)-(-1)^J(y_2+y_3-z)\}$		$\sqrt{2}\{2(1-z)-(-1)^J(y_2+y_3-z)\}$	

Table 14b. Numerators and the additional propagators of the graphs of group 10 with helicity $(-,+,+)$

I.P.	Num. for graphs of Group 10 with $(\lambda_1, \lambda_2, \lambda_3) = (-,+,+)$		X-Prop.
	$J = 1$	$J = 2$	
U3	$(-1)^J\sqrt{2}z(y_2+y_3-z)(2x_2+x_3-z)$		$\frac{1}{-z(x_3-z)(2m_c)^2}$
L3	$\emptyset$	$\emptyset$	n.g.
U2	$(-1)^J\sqrt{2}z(y_2+y_3-z)(2x_3+x_2-z)$		$\frac{1}{-z(y_3-z)(2m_c)^2}$
L2	$\emptyset$	$\emptyset$	n.g.
U1	$\emptyset$	$\emptyset$	n.g.
M1	$\emptyset$	$\emptyset$	n.g.
L1	$\emptyset$	$\emptyset$	n.g.
G3	$(-1)^J\sqrt{2}(y_2+y_3-z)$ $\times(x_3y_2+x_2y_3+x_3y_3+z(x_2+y_2-z))$		$\frac{1}{x_3y_3(2m_c)^2}$
G2	$(-1)^J\sqrt{2}(y_2+y_3-z)$ $\times(x_3y_2+x_2y_3+x_2y_2+z(x_3+y_3-z))$		$\frac{1}{x_2y_2(2m_c)^2}$
GR	$\emptyset$	$\emptyset$	n.g.
4G	$(-1)^J 2\sqrt{2}(y_2+y_3-z)$		$\frac{1}{(2m_c)^2}$

B Numerical parameters

Here we gather together our input as well as other parameters used in the calculations in table form.

B.1 Basic parameters

Table 15. Basic input parameters

Symbol	Value
Λ_{QCD}	0.22GeV
m_c	1.50GeV
μ_0	1.00GeV
$\mu_R(\mathrm{SHSA})$	m_c
$\mu_R(\mathrm{MHSA})$	square root of the largest virtuality, see Sect. 6
n_f	4

B.2 Charmonium parameters

Table 16. Charmonium parameters

Symbol	Value	Origin
$|R'_{\mathrm{P}}(0)|$	$0.220\mathrm{GeV}^{5/2}$	see [20,37]
$f^{(8)}_{\chi_1}$	$0.225 \times 10^{-3}\mathrm{GeV}^2$	*obtained from fit here*
$f^{(8)}_{\chi_2}$	$0.900 \times 10^{-3}\mathrm{GeV}^2$	from [20]
$z = z_3$	0.150	from [20,21]
$z_1 = z_2 = (1-z)/2$	0.425	from [20,21]

B.3 Baryon wavefunction parameters

Table 17. Baryon wave function parameters derived in [11] with the constituent strange quark mass $m_s = 350\,\mathrm{MeV}$, the octet baryon decay constant $f_{B_8} = 6.64 \times 10^{-3}\,\mathrm{GeV}^2$ and the transverse size parameter $a_{B_8} = 0.75\,\mathrm{GeV}^{-1}$ at the reference scale μ_0. The same for the decuplet baryons are $f_{B_{10}} = 0.0143\,\mathrm{GeV}^2$ and $a_{B_{10}} = 0.80\,\mathrm{GeV}^{-1}$. Note that in [11] of all the decuplet baryons, only the parameters of Δ were given

Baryon	B_1	B_2	B_3	B_4	B_5
N	0.750	0.250	0.000	0.000	0.000
Σ	0.216	0.394	−0.293	−0.914	0.241
Ξ	1.106	0.050	−0.282	1.717	−0.498
Λ	−0.721	0.389	−0.150	−0.574	0.093
Δ	0.000	0.000	0.000	0.000	0.000
Σ^*	−0.547	0.182	−0.216	−1.081	0.062
Ξ^*	0.540	−0.180	−0.382	1.742	−0.413

From these parameters, the mean squared internal transverse momentum of the baryons $\rho^2 = \langle \boldsymbol{k}_\perp{}^2 \rangle$ can be worked out. The average value is $\rho_{(8)} = 415.0\,\mathrm{MeV}$ for the octet and $\rho_{(10)} = 389.0\,\mathrm{MeV}$ for the decuplet baryons. Their use as infrared cutoff was discussed in Sect. 8.

References

1. S.J. Brodsky, G.P. Lepage, Phys. Rev. D **22**, 2157 (1980)
2. A. Duncan, A.H. Mueller, Phys. Lett. B **93**, 119 (1980)
3. G.T. Bodwin, E. Braaten, G.P. Lepage, Phys. Rev. D **46**, 1914 (1992)
4. G.T. Bodwin, E. Braaten, G.P. Lepage, Phys. Rev. D **51**, 1125 (1995)
5. V.L. Chernyak, A.R. Zhitnitsky, Nucl. Phys. B **201**, 492 (1982)
6. V.L. Chernyak, A.R. Zhitnitsky, Phys. Rep. **112**, 173 (1984)
7. V.L. Chernyak, A.A. Ogloblin, A.R. Zhitnitsky, Z. Phys. C **42**, 569 (1989)
8. J. Bolz, R. Jakob, P. Kroll, M. Bergmann, N.G. Stefanis, Z. Phys. C **66**, 267 (1995)
9. A.V. Radyushkin, Nucl. Phys. A **532**, 141 (1991)
10. J. Bolz, P. Kroll, Z. Phys. A **356**, 327 (1996)
11. J. Bolz, P. Kroll, Eur. Phys. J. C **2**, 454 (1998)
12. J. Botts, G. Sterman, Nucl. Phys. B **325**, 62 (1989)
13. H.N. Li, G. Sterman, Nucl. Phys. B **381**, 129 (1992)
14. S.M.H. Wong, preprint NUC-MINN-98/11-T, hep-ph/9903221, to appear in Nucl. Phys. A
15. M. Gari, N.G. Stefanis, Phys. Rev. D **35**, 1074 (1987)
16. I.D. King, C.T. Sachrajda, Nucl. Phys. B **279**, 785 (1987)
17. M. Bergmann, N.G. Stefanis, Phys. Rev. D **47**, 3685 (1993)
18. Z. Dziembowski, Phys. Rev. D **37**, 768 (1988)
19. S.J. Brodsky, G.P. Lepage, Phys. Rev. D **24**, 2848 (1981)
20. J. Bolz, P. Kroll, G.A. Schuler, Phys. Lett. B **392**, 198 (1997)
21. J. Bolz, P. Kroll, G.A. Schuler, Eur. Phys. J. C **2**, 705 (1998)
22. F. Murgia, M. Melis, Phys. Rev. D **54**, 3365 (1996)
23. R.M. Barnett et al, Phys. Rev. D **54**, 1 (1996)
24. A. Andrikopoulou, Z. Phys. C **22**, 63 (1984)
25. P.H. Damgaard, K. Tsokos, E.L. Berger, Nucl. Phys. B **259**, 285 (1985)
26. V.L. Chernyak, A.A. Ogloblin, A.R. Zhitnitsky, Z. Phys. C **42**, 583 (1989)
27. F. Murgia, M. Melis, Phys. Rev. D **51**, 3487 (1995)
28. V.A. Novikov, L.B. Okun, M.A. Shifman, A.I. Vainshtein, M.B. Woloshin, V.I. Zakharov, Phys. Rep. **41**, 1 (1978)
29. J.Z. Bai et al, BES Collaboration, Phys. Rev. Lett. **81**, 3091 (1998)
30. P. Kroll, S.M.H. Wong, in Proceedings of the IVth International Workshop on Progress in Heavy Quark Physics, Rostock, Germany, 1997, edited by M. Beyer, T. Mannel, H. Schröder (Rostock University Press 1998), p. 185
31. G. Grunberg, Phys. Lett. B **327**, 121 (1996)
32. Yu.L. Dokshitzer, V.A. Khoze, S.I. Troyan, Phys. Rev. D **53**, 89 (1996)
33. D.V. Shirkov, I.L. Solovtsov, Phys. Rev. Lett. **79**, 1209 (1997)
34. B.R. Webber, JHEP **10**, 012 (1998)
35. S.M.H. Wong, work in progress
36. H.Ch. Kim, W. Schroers, N.G. Stefanis, preprint RUB-TPII-17/98, PNU-NTG-04/98, hep-ph/9812280
37. M.L. Mangano, A. Petrelli, Phys. Lett. B **352**, 445 (1995)